Comparison of model and ground observations finds snowpack and blowing snow aerosols both contribute to Arctic tropospheric reactive bromine

William F. Swanson[1], Chris D. Holmes[2], William R. Simpson[1], Kaitlyn Confer[3], Louis Marelle[4,5], Jennie L. Thomas[4], Lyatt Jaeglé[3], Becky Alexander[3], Shuting Zhai[3], Qianjie Chen[6], Xuan Wang[7], Tomás Sherwen[8,9]

[1]Department of Chemistry and Biochemistry and Geophysical Institute, University of Alaska Fairbanks, Fairbanks, Alaska

[2]Department of Earth, Ocean and Atmospheric Science, Florida State University, Tallahassee, Florida

[3]Department of Atmospheric Sciences, University of Washington, Seattle, Washington

[4]Institut des Géosciences de l'Environnement (IGE), Institut Polytechnique de Grenoble, Grenoble, France

[5]Laboratoire Atmosphères Observations Spatiales (LATMOS), Sorbonne Université, Paris, France

[6]Department of Civil and Environmental Engineering, Hong Kong Polytechnic University, Hong Kong, China

[7]School of Energy and the Environment, City University of Hong Kong, Hong Kong, China

[8]National Centre for Atmospheric Science, University of York, York, UK.

[9]Department of Chemistry, University of York, York, United Kingdom

Correspondence to: William F. Swanson (wswanson3@alaska.edu)

Abstract

Reactive halogens play a prominent role in the atmospheric chemistry of the Arctic during springtime. Field measurements and modelings studies suggest that halogens are emitted to the atmosphere from snowpack and reactions on wind-blown snow and aerosols. The relative importance of snowpack and blowing snow sources is still debated, both at local scales and regionally throughout the Arctic. To understand implications of these halogen sources on a pan-Arctic scale, we simulate Arctic reactive bromine chemistry in the atmospheric chemical transport model GEOS-Chem. Two mechanisms are included: 1) a blowing snow sea salt aerosol formation mechanism and 2) a snowpack mechanism assuming uniform molecular bromine production from all snow surfaces. We compare simulations including neither mechanism, each mechanism individually, and both mechanisms to examine conditions where one process may dominate or the mechanisms may interact. We compare the models using these mechanisms to observations of bromine monoxide (BrO) derived from multiple-axis differential optical absorption spectroscopy (MAX-DOAS) instruments on O-Buoy platforms on the sea ice and at a coastal site in Utqiaġvik, Alaska during spring 2015. Model estimations of hourly and monthly average BrO are improved by assuming a constant yield of 0.1% molecular bromine from all snowpack surfaces on ozone deposition. The blowing snow mechanism increases modeled BrO by providing more bromide-rich

aerosol surface area for reactive bromine recycling. The snowpack mechanism led to increased model BrO across the Arctic Ocean with maximum production in coastal regions, whereas the blowing snow mechanism increases BrO in specific areas due to high surface windspeedwind speeds. Our uniform snowpack source has a greater impact on BrO mixing ratios than the blowing snow source. Model results best replicate several features of BrO observations during spring 2015 when using both mechanisms in conjunction, adding evidence that these mechanisms are both active during the Arctic Spring. Extending our transport model throughout the entire year leads to predictions of enhanced fall BrO that are not supported by observations.

1. Introduction

Simulating Arctic halogen chemistry is a persistent problem for global models because processes appear to differ between the Arctic and middle latitudes (Parrella et al., 2012; Schmidt et al., 2016). Space-based instruments observe large column densities of reactive bromine across swaths of the Arctic Ocean during the Arctic spring (Chance, 1998; Richter et al., 1998; Wagner and Platt, 1998). Increased levels of tropospheric reactive bromine are associated with ozone depletion events (Barrie et al., 1988; Foster et al., 2001; Koo et al., 2012; Halfacre et al., 2014) as well as oxidation of gaseous elemental mercury (Schroeder et al., 1998; Nghiem, 2013; Moore et al., 2014). Bromine radicals have been observed to lead directly to ozone depletion and mercury oxidation (Wang et al., 2019a). Deposition of oxidized mercury to the snowpack can have deleterious effects on the health of Arctic humans and animals (AMAP, 2011). Arctic reactive bromine chemistry impacts tropospheric oxidative chemistry but is not typically accounted for in global models. Model studies have found that reactive halogen chemistry can explain the oxidation of gaseous elemental mercury (Holmes et al., 2010) and reduce radiative forcing from ozone (Sherwen et al., 2016c). Replicating reactive halogen chemistry in models requires inclusion of multi-phase chemical reactions as well as mechanisms affecting sea salt aerosol particle production and chemical reactions within the snowpack.

These increased levels of tropospheric reactive bromine radicals are a product of heterogeneous photochemical reactions at the interface between air and saline surfaces such as surface snowpack and sea salt aerosols (Saiz-Lopez and von Glasow, 2012; Simpson et al., 2015). Figure 1 depicts the gas-phase, heterogeneous, and photochemical reactions thought to control tropospheric bromine, all of which are included in the model and results presented in this manuscript. Bromine radicals (Br) are produced by photolysis of molecular bromine (P1) or by self-reaction of BrO (R6) and react with ozone to form bromine monoxide (BrO) (R2). Under sunlit conditions, BrO is most often photolyzed back to Br radicals and an oxygen atom (P2) that then most often reforms ozone, resulting in a null cycle. Due to this rapid interchange of Br and BrO, these two compounds form the BrO_x family. If processes other than BrO

67   photolysis (P2~~1~~) convert BrO back to Br without producing ozone, the imbalance between these other

68   processes and P2~~1~~ result in net ozone depletion. For example, ozone is depleted through R6 or R7 when

69   BrO reacts with another halogen oxide to form either Br_2 or BrCl, or through other more extended

70   processes. A reactive halogen activating cycle occurs when a BrO radical reacts with a hydroperoxy

71   (HO_2) radical in R5 to form gaseous hypobromous acid (HOBr). Heterogeneous chemistry can occur on a

72   saline surface between HOBr and particulate bromide (p-Br$^-$) in HR1 forming Br_2 or particle chloride (p-

73   Cl$^-$) in HR6 forming BrCl. For each cycle of reactions P1, R2, R5, and HR1, one hydroperoxy radical is

74   removed from the atmosphere, one bromine atom~~radical~~ is released to the atmosphere, and one ozone

75   molecule is destroyed. This process of activation of particulate bromide to Br_2 by consuming other

76   radicals (e.g. HO_2) is known as the "bromine explosion" (Wennberg, 1999). Ground-based instruments

77   have observed sharp increases in reactive bromine levels over the course of a single day from below 2

78   pmol/mol up to a maximum of 41 pmol/mol (Pöhler et al., 2010). Reactions may also sequester reactive

79   bromine into more stable bromine reservoir species. BrO may react with nitrogen dioxide (NO_2) in R8 to

80   form bromine nitrate ($BrNO_3$), which can also undergo hydrolysis on ~~a saline~~aqueous and ice surface~~s~~ to

81   form HOBr as in HR3.
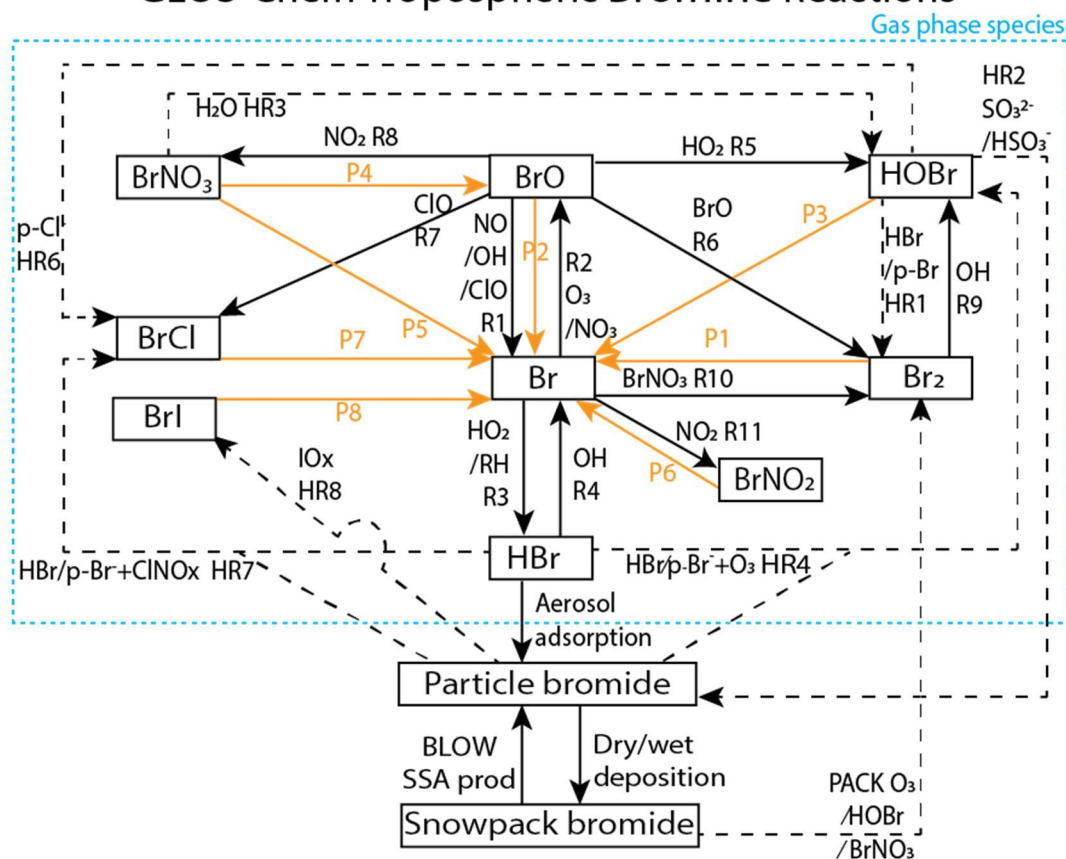
GEOS-Chem Tropospheric Bromine Reactions

83
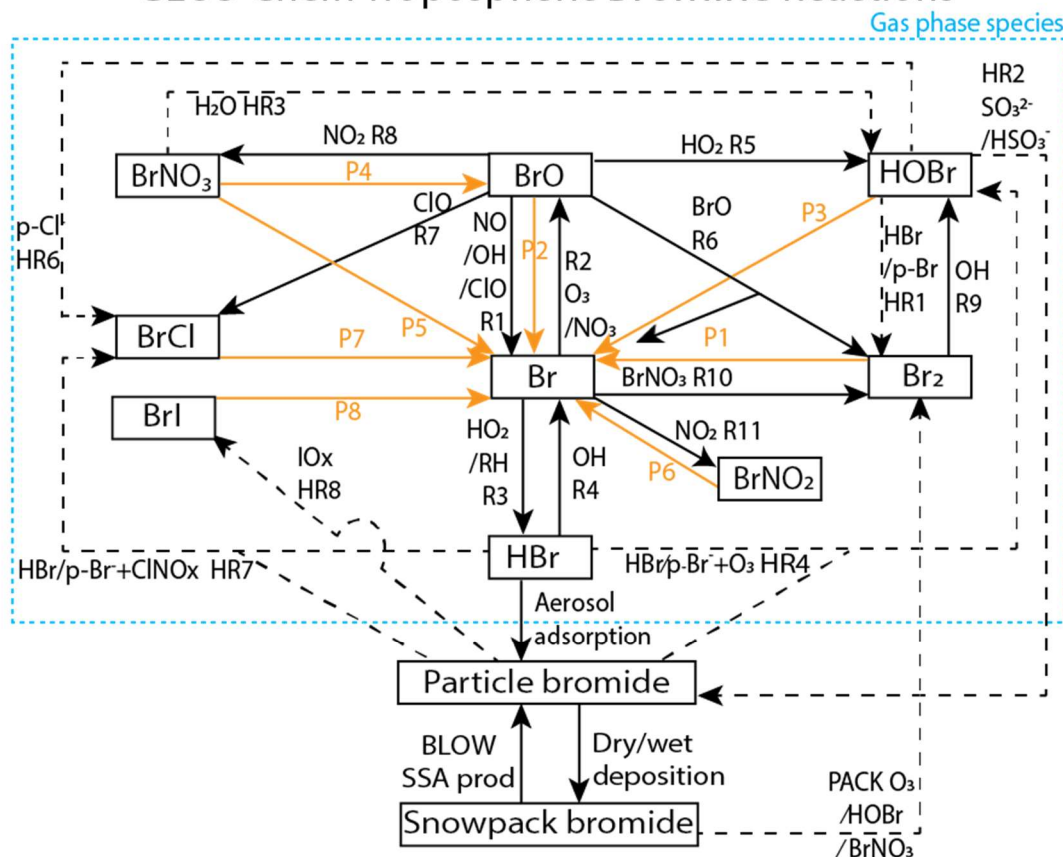
Figure 1: GEOS-Chem tropospheric bromine reactions. Tropospheric bromide reservoirs shown in
black boxes, with attached lines indicating reactions. Solid black lines R1-R11 indicate gas phase
chemical reactions, solid orange lines P1-P8 indicate photolysis reactions, and dashed black lines HR1-
HR8 indicate heterogeneous reactions. All gaseous species may undergo ~~wet and~~ dry deposition.
Additional sources of tropospheric bromine include the production of particulate bromide by the BLOW
mechanisms and the production of Br_2 by the PACK mechanism, as well as the degradation of
organobromines to form Br (OR1). Table 3 enumerates the specific species involved in each equation and
shows reaction rates for each respective equation.

A potentially important competitor for recycling of reactive bromine through HOBr is its reaction
with sulfur (IV) species, such as the reaction between HSO_3^- and HOBr in HR2 (Chen et al., 2017). To
the extent that this reaction competes with HR1, it can slow the release of bromide from surfaces and
reduce gas-phase reactive bromine (e.g., reduce BrO). Deposition of the HBr formed from HOBr by HR2
can remove reactive bromine from the troposphere. In general, the termination of this chemistry leads to
formation of HBr, which undergoes gas-particulate uptake to particulate bromide (p-Br⁻).

98   Ozone deposited to a saline surface can oxidize Br^- to form HOBr (similar to p-Br^- reactions

99   HR4a and HR4b) which is then converted to Br_2 or another dihalogen (e.g., BrCl). Production of reactive

100   bromine during ozone deposition does not require light and can occur at night (Oum et al., 1998; Artiglia

101   et al., 2017). The production of Br_2 is increased at low pH levels (Halfacre et al., 2019).

102   We define the inorganic bromine family, Br_y, in this manuscript as the sum of the bromine

103   species: Br, BrO, HOBr, $BrNO_3$, $2xBr_2$, BrCl, BrI, and HBr, excluding p-Br^-. The release of bromine from

104   sea salt aerosol particles was found to be the dominant global source of reactive bromine (Sander et al.,

105   2003; Zhu et al., 2019). Sea salt aerosol particles (SSA) sourced from the bursting of bubbles in oceanic

106   whitecaps and other sources and are one of the most abundant aerosol particle types present in the

107   troposphere (De Leeuw et al., 2011). Due to their abundance, SSA particles greatly increase the ~~surface~~

108   ~~area~~particulate bromide on aerosol surfaces available for heterogeneous reactive bromine chemistry .

109   Debromination of acidified aerosol increases reactive bromine by 30%, although global models may

110   underestimate Arctic reactive bromine when considering only open ocean-sourced SSA (Schmidt et al.,

111   2016). Initial literature on Arctic reactive bromine chemistry identified aerosol particles as a potential

112   saline surface for reactive bromine photochemistry (Fan and Jacob, 1992; Vogt et al., 1996) and recent

113   studies confirmed that SSA is depleted in bromide (Hara et al., 2018). If one supposes that SSA can only

114   be produced from the open ocean source of SSA, the lack of Arctic Ocean open water during the

115   winter/spring is at odds with observations of high SSA concentrations observed during the winter months

116   in polar regions (Wagenbach et al., 1998; Huang et al., 2018). The formation of SSA from the sublimation

117   of blowing snow particles over the Arctic Ocean was proposed as an alternate SSA production

118   mechanism (Yang et al., 2008, 2010, 2019). Recent field studies have confirmed the direct production of

119   SSA from blowing snow (Frey et al., 2020). A blowing snow SSA mechanism was implemented in the

120   global chemical model GEOS-Chem and was able to explain wintertime SSA enhancements over the

121   Arctic (Huang and Jaeglé, 2017) as well as CALIOP-detected aerosol particle abundance (Huang et al.,

122   2018) and high levels of Arctic BrO detected by satellites in spring (Huang et al., 2020).

123   Snowpack containing bromide salts was also identified as a source of reactive bromine (Tang and

124   McConnell, 1996). Molecular bromine was measured above the snowpack at levels up to 25 pmol/mol

125   (Foster et al., 2001). Field experiments demonstrate that the snowpack emits Br_2, Cl_2, and BrCl, with

126   emission affected by ambient ozone levels, the snowpack ratio of bromide to chloride, and exposure to

127   sunlight (Pratt et al., 2013; Custard et al., 2017). Box modeling found that the flux of reactive bromine

128   from the surface of the Arctic Ocean sea ice is a prerequisite for bromine activation (Lehrer et al., 2004).

129   Box modeling found that both HOBr and $BrNO_3$ can be converted to Br_2 in the snowpack (Wang and

130   Pratt, 2017). Detailed one dimensional models of the snowpack-air interface find that reactive bromine

131   production can occur in the interstitial air between snowpack grains (Thomas et al., 2011; Toyota et al.,

132   2014), with ozone depletion events arising from snowpack reactive bromine production (Thomas et al.,

133   2011; Toyota et al., 2014; Cao et al., 2016). However, a detailed snowpack model coupled to an

134   atmospheric model would be sensitive to important parameters such as snowpack bromide content and

135   acidity of the air-ice interface that are highly variable across the Arctic (Toom-Sauntry and Barrie, 2002;

136   Krnavek et al., 2012). A mechanism to parameterize the release of molecular bromine from snowpack

137   upon deposition of ozone, HOBr, and $BrNO_3$ was implemented in the GEM-AQ model and captured

138   many of the observed features of reactive bromine in the Arctic troposphere (Toyota et al., 2011). The

139   mechanisms from Toyota et al. (2011) assumes a 100% yield of molecular bromine on deposition of

140   HOBr or $BrNO_3$ (see Figure 1 PACK) and a diurnally varying yield of Br_2 on ozone deposition of 7.5%

141   during the daytime (solar elevation angle > 5°) and 0.1% during the nighttime (solar elevation angle < 5°)

142   (see Figure 1 PACK). In the Toyota et al. (2011) parameterization, the daytime yield of Br_2 from ozone

143   was increased to 7.5% to match surface ozone depletion observations and is based on the assumption that

144   photochemical reactions in the snowpack would trigger a bromine explosion and amplify the net release

145   of Br_2 (Toyota et al., 2011). Herrmann et al (2021) implemented the Toyota et al. (2011) mechanism in

146   WRF-Chem and found snowpack Br_2 production was capable of replicating ozone depletion events

147   observed in multiple datasets. Marelle et al. (2021) implemented a surface snowpack mechanism based on

148   Toyota et al. (2011) and a blowing snow SSA mechanism based on Yang et al. (2008) and Huang and

149   Jaeglé (2017) and found improved prediction of ozone depletion events, the majority of which were

150   triggered by the snowpack mechanism. The Toyota et al. (2011) mechanism was also implemented in the

151   EMAC model and replicated many of the features of reactive bromine events observed by satellite-based

152   GOME sensor (Falk and Sinnhuber, 2018).

153   Field campaigns have directly observed the production of SSA from blowing snow (Frey et al.,

154   2020) as well as production of Br_2 from the snowpack (Pratt et al., 2013) in the environment. This

155   manuscript uses both production mechanisms for the first time in the global chemical model GEOS-

156   Chem. We devised a set of six model runs to test each mechanism individually and together as well as one

157   control run using neither mechanism. We compare BrO simulated in each model run against extensive

158   ground-based observations of BrO made from February to June 2015. This set of modeling scenarios

159   allows identification of the effects of each mechanism on BrO as well as the synergistic effects of both

160   mechanisms working together.

2. Data sources and methods

2.1 MAX-DOAS observation platforms

Multiple axis differential optical absorption spectroscopy (MAX-DOAS) remotely measures the vertical profile of BrO (Hönninger and Platt, 2002; Carlson et al., 2010; Frieβ et al., 2011; Peterson et al., 2015; Simpson et al., 2017). BrO is commonly used as a proxy for total tropospheric reactive bromine (Chance, 1998; Richter et al., 1998; Wagner and Platt, 1998; Theys et al., 2011; Choi et al., 2012). MAX-DOAS instruments were mounted on all of the fifteen floating autonomous platforms (O-Buoys) deployed in the Arctic sea ice as a part of the National Science Foundation-funded Arctic Observing Network project (Knepp et al., 2010). Since MAX-DOAS requires sunlight to operate, measurements are not available in winter. Spring observations on the O-Buoys typically begin in April when there is enough O-Buoy solar power to defrost the MAX-DOAS viewport. Figure 2 shows the O-Buoys active during 2015. O-Buoy 10 was deployed into sea ice in fall 2013 and measured reactive halogen chemistry in spring 2014 and 2015. Most O-Buoys were destroyed in the summer, crushed between fragments of melting sea ice. However, O-Buoy 10 survived summer 2014 in an intact ice floe, survived the winter of 2014-15, and re-started MAX-DOAS observations in April 2015. O-Buoys 11 and 12 were deployed in fall 2014 and also re-started observing BrO in April 2015. Figure 2 shows the GPS-derived tracks of the O-Buoys for their full deployment and highlights the O-Buoy locations from April to June 2015 when the BrO observations considered in this analysis were gathered. A MAX-DOAS instrument of the same design was deployed at the Barrow Arctic Research Center (BARC) on the coast of the Arctic Ocean located at 156.6679°W, 71.3249°N near Utqiaġvik, AK (Simpson, 2018), also shown in Figure 2. Unlike the O-Buoy MAX-DOAS systems, which were powered by batteries and solar panels, the BARC MAX-DOAS was powered from local utilities and was able to defrost its viewport to gather BrO observations earlier in the year, including February and March 2015. The BARC MAX-DOAS data was compared with two O-Buoy style MAX-DOAS instruments deployed on Icelander platforms (deployed on top of sea ice instead of within) and measurements from the various MAX-DOAS systems were found to be comparable (Simpson et al., 2017). The reactive bromine season ends when the BrO slant column densities fall below the instrument detection limit and do not recover, which we call the seasonal end date (Burd et al., 2017). All O-Buoy and BARC (Utqiaġvik) data are available at arcticdata.io (Simpson et al., 2009) (Simpson, 2018). More information on the time periods of spring BrO observations can be found in Swanson et al. (2020) and Burd et al. (2017). For comparison to the MAX-DOAS BrO observations, GEOS-Chem model simulations are sampled along the GPS-derived paths of O-Buoys 10, 11 and 12 as well as at BARC.

192
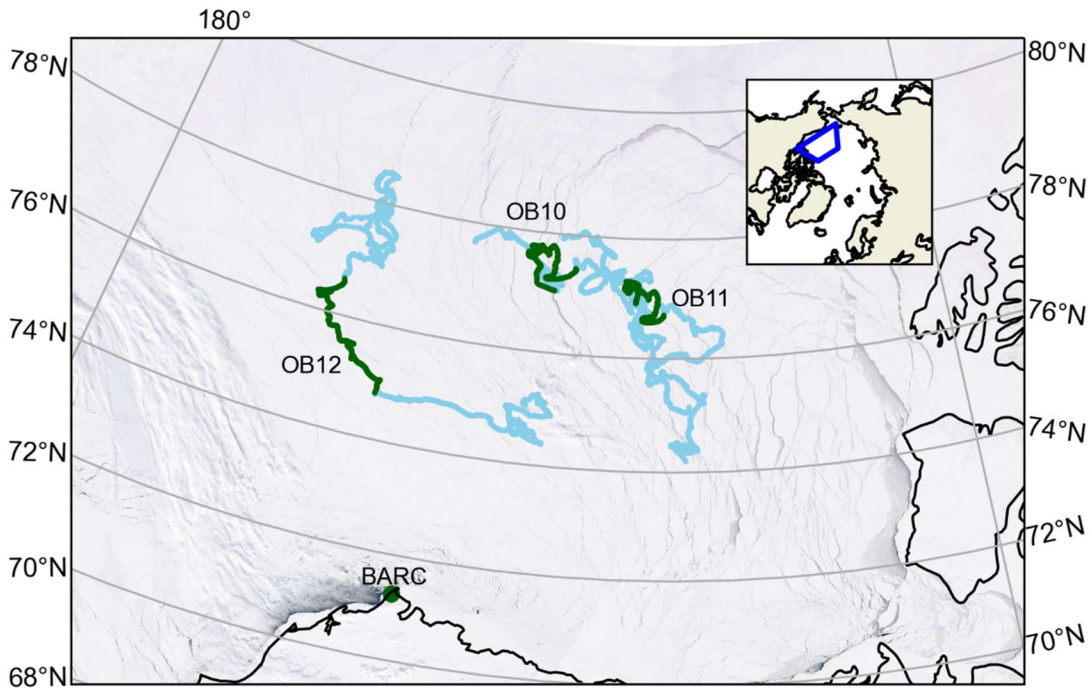
Figure 2: Locations of MAX-DOAS BrO observations used in this work.
Blue lines show the drift tracks of O-Buoys, with green showing the locations with valid BrO
measurements in spring 2015. Location of Barrow Arctic Research Center (BARC) in Utqiaġvik indicated
by green dot. ~~Inset map shows~~ True color MODIS imagery on 1 April 2015 shows typical sea ice
coverage (NASA 2015). Inset map shows location of map grid within northern hemisphere.

2.2 MAX-DOAS profile retrieval

Vertical profiles of BrO were derived from MAX-DOAS observations by means of optimal estimation inversion procedures detailed in Peterson et al. (2015) with settings detailed in Simpson et al. (2017). The HeiPro optimal estimation algorithm (Frieß et al., 2006, 2019) is used to retrieve a vertical profiles of BrO between the surface and 4km from the MAX-DOAS observations. Examination of the averaging kernels from each MAX-DOAS retrieval finds the retrieved vertical profile of BrO is best represented by two quantities: the vertical column density of BrO in the lowest 200 m, and the vertical column density of BrO in the lowest 2000 m of the troposphere referred to in this manuscript as BrO_{LTcol} (Peterson et al., 2015). ~~We approximate surface mixing ratio by assuming well mixed constant distribution of BrO throughout the lowest 200 m. This mixing ratio is reported as $BrO_{pptv200}$ (Simpson et al 2009, Simpson 2018).~~ It was shown in Peterson et al. (2015) that these two quantities were largely independent of each other, were fairly insensitive to variations in the assumed prior profile, and represented the ~2-3 degrees of freedom for signal indicated by the optimal estimation retrieval. An important consideration of this method is that when the visibility is poor, the MAX-DOAS is unable to traverse the lowest 2000m AGL and the BrO_{LTcol} cannot be measured accurately. Therefore, our quality-control algorithm eliminates BrO_{LTcol} observations when the degrees of freedom for signal in the lofted (200m - 2000m AGL) layer were below 0.5 (Simpson et al., 2017). The average fitting error (1σ error) of BrO_{LTcol} during spring 2015 was $5.6*10^{12}$ molecules/cm².

2.3 SSA production from open ocean

Seafoam from breaking waves and bursting of bubbles forms aerosol droplets suspended in the marine boundary layer (Lewis and Schwartz, 2004). We calculate emission of sea salt aerosol particles from the open ocean as a function of wind speed and sea surface temperature (SST) using the mechanism initially described in Jaeglé et al. (2011) and updated with decreased emissions over cold (SST < 5°C) ocean waters (Huang and Jaeglé, 2017). Two separate SSA tracers are transported: accumulation mode SSA (r_{dry} = 0.01−0.5 µm) and coarse mode SSA (r_{dry} = 0.5–8 µm). Sea salt bromide is emitted assuming bromine content of 2.11×10^{-3} kg Br per kg of dry SSA (primarily NaCl) based on the mean ionic composition of sea water (Sander et al., 2003). Bromide content is tracked separately on accumulation mode SSA and on coarse mode SSA. Freshly emitted SSA is alkaline and can be titrated to a pH of 5 by uptake of acid gases SO_2, H_2SO_4, and HNO_3 (Alexander et al., 2005). Heterogeneous chemical reactions can convert SSA-transported bromide into gaseous reactive bromine species in the atmosphere. We run our open ocean SSA calculations at 0.5° latitude x 0.625° longitude spatial resolution using the harmonized emissions component (HEMCO) for highest possible detail (Keller et al., 2014; Lin et al., 2021) including cold water corrections used in Jaeglé et al. (2011) . Production of SSA from open oceans ~~which can lead to Arctic reactive bromine recycling on advected open ocean SSA within GEOS-Chem~~

232   followed by advection can lead to reactive bromine recycling over Arctic Ocean sea ice. Each of our

233   model runs reads the dataset generated offline by HEMCO rather than spend computational time

234   replicating open ocean SSA emissions. We call our control run using only open ocean SSA emissions

235   BASE.

2.4 Blowing snow SSA production

237   Snow can be lofted from the snowpack into the lowest layers of the troposphere by high

238   ~~windspeed~~wind speeds, where it can undergo saltation (bouncing leading to fragmentation) and

239   sublimation to form SSA (Yang et al., 2008, 2010; Frey et al., 2020). This process is modeled as a

240   function of humidity, ambient temperature, ~~windspeed~~wind speed, and the salinity of the blowing snow

241   (Yang et al., 2008, 2010). We assume that snowpack exists on all sea ice surfaces during the Arctic

242   Spring after snow accumulation during winter on sea ice of all ages. Three thresholds must be met for

243   SSA production from blowing snow (Dery and Yau, 1999; Déry and Yau, 2001). A temperature threshold

244   restricts SSA production from blowing snow to temperatures below freezing. The humidity threshold is

245   based on relative humidity with respect to ice. Sublimation from snow crystals cannot occur if the air is

246   saturated, and no SSA is produced if RH_{ice} is greater than 100%. The ~~windspeed~~wind speed threshold

247   requires ~~ten-meter~~10-m wind speed to be greater than a threshold value defined in Equation 1 for any

248   production of SSA (Dery and Yau, 1999; Déry and Yau, 2001).

249    $$U_t = 6.975 + 0.0033(T_s + 27.27)^2 \tag{1}$$

250   The wind speed threshold (U_t) is dependent on surface temperature (T_s) in Celsius with a minimum

251   threshold of 6.975 m/s at -27.27 °C~~C°~~ and a maximum threshold at 0 °C~~C°~~ of 9.429 m/s. The ~~ten-meter~~10-

252   m ~~windspeed~~wind speed threshold is the most stringent and often controls the production of SSA from

253   blowing snow.

254   Production of blowing snow ~~and~~ SSA is highly sensitive to surface ~~windspeed~~wind speed. We

255   use the highest resolution surface ~~windspeed~~wind speed dataset to ensure the most accurate modeling of

256   SSA and reactive bromine. The MERRA-2 Global Reanalysis Product has a 0.5° latitude x 0.625°

257   longitude resolution which is typically re-gridded to a lower resolution for global chemical modeling.

258   Previous use of the snowpack blowing snow SSA mechanism ~~has simulated blowing snow~~used ~~with~~

259   MERRA-2 data re-gridded to either 2°x2.5° or 4°x5° latitude and longitude (Huang and Jaeglé, 2017;

260   Huang et al., 2018, 2020). Re-gridding to coarser spatial resolution may smooth out the highest ~~ten-~~

261   ~~meter~~10-m ~~windspeed~~wind speeds by averaging them with lower ~~windspeed~~wind speeds in the grid cell.

262   The Utqiaġvik MERRA-2 ~~ten-meter~~10-m ~~windspeed~~wind speeds at different spatial resolutions are

263   shown in Supplemental Figures S1, S2 and S3 to illustrate this effect. Average Utqiaġvik ~~ten-meter~~10-m

264   ~~windspeed~~wind speeds for 2015 are 5.3 m/s at 2°x2.5° resolution and 5.5 m/s at 0.5°x0.625° resolution.

265 The maximum Utqiaġvik 10-m ~~ten meter windspeed~~wind speed at MERRA-2 2x2.5 is 16.3 m/s, while the

266 maximum ~~windspeed~~wind speed at MERRA-2 0.5°x0.625° is 19.3 m/s. These extremely high

267 ~~windspeed~~wind speed events are more common at higher spatial resolution and can contribute an outsized

268 amount of SSA to the marine boundary layer. Supplemental Figure S4 shows the measured ~~ten-meter~~10-

269 m ~~windspeed~~wind speed at BARC, along with daily average threshold ~~windspeed~~wind speed (Equation

270 1). Spikes in daily averaged ~~windspeed~~wind speed at BARC in April can contribute to SSA formation and

271 justify the use of high-resolution MERRA-2 wind speed data.

272   Snow salinity is influenced by snow age and the material underlying the snow (Krnavek et al.,

273 2012). The median surface snowpack salinity near Utqiaġvik was measured at 0.67 practical salinity units

274 (PSU)PSU for 2-3 weeks old sea ice, 0.12 PSU for thicker first year ice, and 0.01 PSU for multi-year ice

275 (MYI) (Krnavek et al., 2012). Snow salinity is also a function of snow depth above sea ice, with blowing

276 surface snow having much lower salinity than snow at depth that is in contact with the sea ice (Frey et al.,

277 2020). Domine et al. (2004) measured median salinity at 0.1 PSU on snowpack over first year ice and

278 0.02 PSU on snowpack over multi-year ice. In this analysis we use a salinity of 0.1 PSU on first-year sea

279 ice as in Huang et al. (2020). The production of reactive bromine from sea ice types is entirely dependent

280 on PSU in this parameterization. Previous modeling efforts have used 0.01 PSU for MYI (Huang et al.,

281 2018) and underestimate BrO production in high Arctic areas with increased MYI coverage. The bromide

282 content of surface snow over MYI is enriched by deposition of SSA and trace gases, and MYI regions

283 may play a role in springtime halogen chemistry (Peterson et al., 2019). Previous analysis of O-Buoy data

284 found no statistically significant differences in springtime BrO between regions of the Arctic (Swanson et

285 al., 2020). We use 0.05 PSU for snowpack on MYI as in Huang et al. (2020).

286   Another important parameter for SSA formation is the number of SSA particles formed from each

287 blowing snowflake. A value of 5 particles per snowflake was used in Huang and Jaeglé (2017) based on

288 wintertime observations of supermicron and sub-micron SSA at Barrow. Values of 1 and 20 particles per

289 snowflake have been tested (Yang et al., 2019) but it is unclear which value was more realistic. We use a

290 particle formation value of 5 particles per snow grain as in Huang et al. (2020).

291   Snowpack may be enriched or depleted in bromide compared to seawater, which is thought to be

292 an effect of atmospheric deposition or release of bromine from snowpack (Krnavek et al., 2012).

293 Snowpack enrichment due to atmospheric deposition is less pronounced when snowpack salinity is high,

294 with snowpack containing 1000 μM Na$^+$ (approximately 0.06 PSU) or more never exceeding twice the

295 seawater ratio of bromine to chloride (Krnavek et al., 2012). Domine et al. (2004) found an increased

296 enrichment factor of five times seawater in snow with a salinity of 100 μM Cl$^-$ (approximately 0.006

297 PSU). We use a snowpack enrichment factor of bromide five times that of seawater as in Huang et al.

298 (2020) where this enrichment best agreed with GOME-2 observations. However, we note that a bromide

299 enrichment factors five times seawater exceeds enrichment factors of two measured in snowpack with a

300 salinity of 0.1 PSU (Krnavek et al., 2012).

301   Our choice of model input settings is similar to Huang et al. (2020) but we will be running the

302 blowing snow SSA mechanism in HEMCO at a 0.5° latitude x 0.625° longitude spatial resolution. The

303 model run using the results of our high-resolution blowing snow SSA HEMCO simulation is called

304 BLOW.

305 **2.5 Snowpack emissions of molecular bromine**

306   We base our Br_2 emissions scheme on Toyota et al. (2011) and Marelle et al. (2021), which

307 prescribe a yield of Br_2 upon snowpack deposition of ozone, $BrNO_3$ and HOBr. In other modeling studies,

308 this simplified deposition-based mechanism captured the synoptic-scale behavior of reactive bromine

309 production across the Arctic (Toyota et al., 2011; Falk and Sinnhuber, 2018; Herrmann et al., 2021;

310 Marelle et al., 2021). These modeling studies used different yields of Br_2 upon deposition over land

311 snowpack, multi-year ice, and first year ice, restricting the production of molecular bromine from ozone

312 deposition to first year ice surfaces. None of these studies were coupled to a snowpack model tracking

313 snow bromide, and effectively assume an infinite bromide reservoir with Br_2 production limited only by

314 the deposition flux and Br_2 yield.

315   Field studies indicate that snowpack over multi-year ice, first-year ice, and land regions may

316 contribute to reactive bromine chemistry. Krnavek et al. (2012) found snow bromide content spanning six

317 orders of magnitude, with individual samples taken from multi-year ice, first-year ice, and land regions

318 showing variability of up to three orders of magnitude for each region. Analysis of variance in

319 tropospheric BrO from 2011-2016 found no statistically significant differences in tropospheric BrO

320 between different regions of the Arctic (Swanson et al., 2020). Both coastal snowpack and multi-year ice

321 regions may produce reactive bromine. Molecular bromine production has been observed from coastal

322 snowpack on exposure to ozone (Pratt et al., 2013; Custard et al., 2017). Airborne sampling has observed

323 enhanced BrO up to 200 km inland (Peterson et al., 2018). Snow above multi-year sea ice regions is

324 depleted in bromide, indicating that it may play a role in Arctic bromine chemistry (Peterson et al., 2019).

325   Our modeling study tests the hypothesis that all snow has a uniform ability to produce molecular

326 bromine, effectively assuming an infinite bromide reservoir with Br_2 production limited only by the

327 deposition flux. We differ from previous model parameterizations in allowing uniform Br_2 production

328 upon snowpack deposition of ozone, $BrNO_3$ and HOBr over all sea ice surfaces and selected coastal

329 snowpack regions. We expect higher predictions of snowpack molecular bromine production than recent

330   modeling efforts (Herrmann et al., 2021; Marelle et al., 2021) in which ozone deposition over land and

331   multi-year ice surfaces did not produce molecular bromine.

2.5.1 Snowpack Br_2 production over sea ice

333   We assume a uniform production of Br_2 on deposition to snowpack over oceanic ice whether the

334   ice is first-year sea or multi-year sea ice. We use MERRA-2 fractional ocean ice coverage fields, which

335   introduces some artifacts. MERRA-2 classifies the freshwater Great Lakes as ocean, but sea ice and

336   snowpack on those frozen lakes is unlikely to have sufficient bromide to support large Br_2 fluxes due to

337   its distance from the ocean. Therefore, we specifically prohibit snowpack Br_2 emissions in the Great

338   Lakes region (between 41° N and 49° N latitude and 75° W and 93° W longitude). This choice is in

339   agreement with McNamara et al. (2020), who found road salt derived aerosol particles are responsible for

340   80-100% of atmospheric $ClNO_2$ in Michigan with no ~~mention of~~strong indication for a source of reactive

341   halogens from nearby Great Lakes.

2.5.2 Snowpack Br_2 production over land

343   We wish to only enable production of Br_2 over land if the snowpack is sufficiently enriched in

344   bromide. Snowpack over land surfaces and glaciers may be enriched in bromide by oceanic SSA sources

345   (Jacobi et al., 2012, 2019). The distance that SSA may be transported inland from the coast is limited by

346   geographical features such as mountains. Based on direct observations of reactive bromine chemistry up

347   to 200 km from the Alaskan coastline (Peterson et al., 2018), we include unlimited production of Br_2 from

348   specific land grid cells within 200 km of the coast upon deposition of ozone, HOBr, and $BrNO_3$. We only

349   allow the fraction of each grid cell that is within 200 km of the coastline (Group and Stumpf, 2021) to

350   produce molecular bromine. We further restrict snowpack Br_2 emissions to locations that are less than 500

351   m above sea level, because higher elevation locations are unlikely to be enriched by sea spray. This

352   altitude screen eliminates Br_2 emissions from coastal mountains such as the Alaskan Rockies, the Brooks

353   Range in Alaska, and the Scandinavian Mountains as well as from the Greenland Plateau. Halogen

354   chemistry may occur over the Greenland ice sheet (Stutz et al., 2011) contrary to this screen, but this will

355   have minimal impact on the regions of interest in this manuscript.

356   Our final screen is based on the average snow depth in each land grid cell. Both modeling studies

357   (Thomas et al., 2011; Toyota et al., 2014) and field studies (Domine et al., 2004; Pratt et al., 2013;

358   Custard et al., 2017; Frey et al., 2020) agree that bromine chemistry can occur in the better ventilated and

359   illuminated top of the snowpack. Regions with less than 10 cm of snowpack may not have sufficient

360   snow for reactive bromine chemistry, thus we only produce snowpack Br_2 when the average snow depth

361   in a land grid cell is 10 cm or greater. This screen prevents molecular bromine production in the lower

362   latitude regions with minimal snow coverage and is necessary because ozone deposition to plants in

363   snow-free grid cells often exceeds the slow deposition of ozone to snowpack and would not be expected

364   to produce Br_2.

2.5.3 Diurnal yield of Br_2 on ozone deposition

366   We choose two alternate assumptions for the yield of Br_2 during the day. Toyota et al. (2011)

367   initially assumed a constant yield of Br_2 from ozone deposition of 0.1% based on laboratory observations

368   of nighttime bromine activation on ozone deposition (Oum et al., 1998; Wren et al., 2010, 2013) and then

369   adjusted the daytime yield of Br_2 on ozone deposition to 7.5% to better match surface ozone mixing ratios

370   measured at coastal stations. This increased daytime yield value was chosen based on the assumption that

371   photochemistry may trigger an autocatalytic cycle leading to a 75-fold increase in Br_2 yield. The

372   PHOTOPACK runs uses the increased daytime Br_2 yield of 7.5% when the solar elevation angle is 5° or

373   greater. Previous implementations of the snowpack mechanism (Toyota et al., 2011; Herrmann et al.,

374   2021; Marelle et al., 2021) predict ozone deposition velocities over Arctic sea ice on the order of 0.01

375   cm/s. Our model predicts similar ozone deposition rates over polar open ocean of 0.009 cm/s (Pound et

376   al., 2020), but our model currently predicts the deposition velocity of ozone over Arctic sea ice between

377   0.02 cm/s and 0.1 cm/s based on the month (see Supplemental Figure S5), with higher values influenced

378   by proximity to the coast as described in Bariteau et al. (2010). Thus, our PHOTOPACK run may predict

379   much higher Br emissions than previous snowpack predictions despite the same yield values due to

380   differences in deposition. To match out magnitude of Br_2 production with previous implementations of

381   the snowpack mechanism (Toyota et al., 2011; Herrmann et al., 2021; Marelle et al., 2021) we add two

382   PACK runs with a constant Br_2 yield on ozone deposition of 0.1% based on yield values in Toyota et al.

383   (2011). Both PACK and PHOTOPACK runs assume 100% conversion of deposited HOBr and $BrNO_3$ to

384   Br_2. Table 1 shows further model run yield details.

Table 1 Model run settings

386   Sea salt aerosol particles are produced from blowing snow as detailed in Section 2.5. Daytime is defined

387   as when the solar elevation angle is greater than 5°, nighttime is defined as when the solar elevation angle

388   is less than 5°.

Model Run	Blowing snow SSA produced	Millimoles Br yielded per mole O3 deposited (daytime)	Millimoles Br yielded per mole O3 deposited (nighttime)
BASE	FALSE	0	0
BLOW	TRUE	0	0
PACK	FALSE	1	1
BLOW+PACK	TRUE	1	1
PHOTOPACK	FALSE	75	1
BLOW+PHOTOPACK	TRUE	75	1

389

2.6 GEOS-Chem chemistry and transport model

The GEOS-Chem global atmospheric chemistry and transport model (Bey et al., 2001) simulates emissions, transport, and chemistry of atmospheric trace gases and aerosols, including halogens. The chemical mechanism in GEOS-Chem 12.9.3 (http://www.geos-chem.org, last access 29 October 2019, DOI:10.5281/zenodo.3974569) includes HO_x-NO_x-VOC-O_3-halogen-aerosol tropospheric chemistry (Mao et al., 2013; Fischer et al., 2014; Fisher et al., 2016; Travis et al., 2016; Wang et al., 2021). The model has been regularly and consistently updated to reflect current understanding of heterogeneous and gas-phase halogen chemistry.

Halogens in the troposphere may be sourced from photooxidation of halocarbons, emissions of iodine from the ocean surface, downward transport of halogens from the stratosphere, and release of halogens through heterogeneous chemistry on SSA. Figure 1 shows a simplified version of the GEOS-Chem reaction scheme focusing on tropospheric bromine reactions and reservoirs. Heterogeneous reactions for release of reactive bromine from aerosol surfaces were added to GEOS-Chem (Parrella et al., 2012) and have been updated to include multiphase reactions involving cloud aerosols and inter-halogen reactions between bromine, chlorine and iodine species (Schmidt et al., 2016; Sherwen et al., 2016a; Wang et al., 2019b) as well as input from the stratosphere (Eastham et al., 2014). Recent updates also include reactions between sulfur (IV) species and HOBr, which lead to a 50% decrease in Br_y due to the scavenging of HOBr on aerosol surfaces containing sulfur (Chen et al., 2017). These HOBr-sulfur(IV) reactions are critical in moderating tropospheric BrO in the mid latitudes (Zhu et al., 2019). In GEOS-Chem 12.9 the halogen chemical mechanism was modified extensively to include chlorine chemistry as detailed in Wang et al. (2019b) with update halogen-sulfur (IV) rates (Liu et al., 2021) as well as improved cloud pH calculation from Shah et al. (2020). For the simulations here, GEOS-Chem uses the Modern-Era Retrospective Analysis for Research and Applications, version 2 (MERRA-2) assimilated meteorological fields (Gelaro et al., 2017) re-gridded from native resolution of 0.5°x0.625° latitude and longitude to 2°x2.5° using a reduced vertical grid of 47 layers.

We initialize our model in October 2014 from a full-chemistry benchmark file, allowing for 6 months of spinup before our period of interest spanning from March to November 2015. We run six different model simulations with settings detailed in Table 1. The base model (BASE) includes the halogen sources described above but no Arctic-specific halogen sources. The BLOW simulation adds SSA production from blowing snow following Huang et al (2020) but using a more recent version of GEOS-Chem. The PACK simulation adds snowpack Br_2 emissions using a constant yield from O_3 deposition. The PHOTOPACK simulation also emits Br_2 from snowpack but increases the Br_2 yield from

422 O_3 deposition under sunlight. These blowing snow SSA and snowpack sources are combined in the

423 BLOW+PACK and BLOW+PHOTOPACK simulations.

2.7 Comparing GEOS-Chem results to MAX-DOAS vertical column densities

425   GEOS-Chem simulates BrO mixing ratios for each of its 47 atmospheric layers. Reducing the

426 vertical resolution of the more-resolved GEOS-Chem predictions to be comparable to the coarser MAX-

427 DOAS data is necessary for appropriate comparison (Rodgers and Connor, 2003). To compare the

428 GEOS-Chem profiles with these two grid-coarsened quantities, we grid-coarsen the averaging kernels

429 produced by the HeiPro retrieval algorithm using Supplemental Equation S1 from Payne et al. (2009) to

430 the partial column averaging kernels shown in Figure 3. We use the average of all April averaging kernels

431 that pass our quality criteria (>0.5 DOFS in the lofted layer), which generally represents non-cloudy

432 conditions. We calculate modeled BrO_{LTcol} by applying the partial column averaging kernels shown in

433 Figure 3 to the GEOS-Chem modeled vertical BrO profiles.

434   Figure 3 shows the average partial column averaging kernel for the surface layer (0-200m AGL)

435 has near unit sensitivity to BrO at the ground, decaying to about 0.5 at 200m AGL then to zero at about

436 400m AGL, as desired. The sensitivity of the BrO_{LTcol} is near unity from about the surface to 600m AGL,

437 then slowly decays with 0.5 sensitivity at 2000m AGL. The resulting sensitivity to mid-tropospheric BrO

438 means that free-tropospheric BrO produced by the GEOS-Chem model contributes to modeled BrO_{LTcol},

439 albeit at 50% or lower sensitivity, even if the GEOS-Chem-predicted free-tropospheric BrO is above the

440 nominal 2000m top of the integration window. The residual sensitivity of the BrO_{LTcol} averaging kernel

441 above 2000m is caused by the limited ability of ground-based MAX-DOAS to distinguish the true altitude

442 of BrO at non-tangent geometries (higher viewing elevation angles) that are required to view BrO at these

443 higher altitudes. Figure 3 shows that BrO above 4 km makes only a small contribution to the modeled

444 BrO_{LTcol}, which was not included in the BrO_{LTcol}.

445
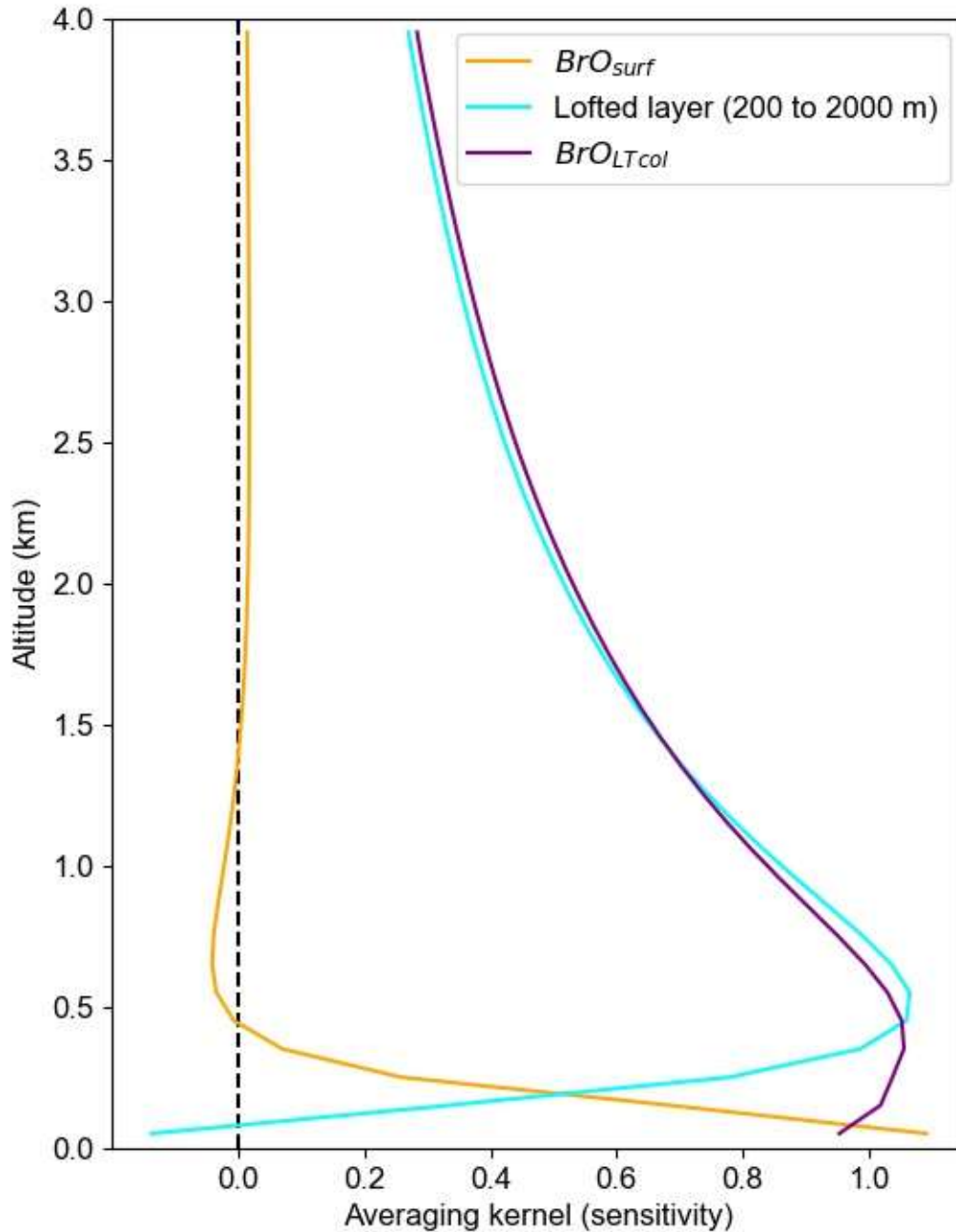
Figure 3: Averaging kernels showing the sensitivity of retrieved BrO$_{LTcol}$ and retrieved BrO$_{surf}$ to BrO at a range of altitudes.

Each line represents a row of the averaging kernel matrix. BrO$_{surf}$ is the column from the surface to 200 m and BrO$_{LTcol}$ is the column up to 2000 m.

Although it has been suggested in the literature (von Clarmann and Glatthor, 2019) that averaged averaging kernels can cause problems, we do not report data when there are clouds and thus are only using the more consistent averaging kernels that occur under clear sky conditions. We use other criteria related to vertical visibility to identify clear skies. As described in Peterson et al. (2015), the information content (DOFS) in the lofted layer is nearly linearly related to the aerosol optical depth. We find that the

455 slant column density of the O$_2$-O$_2$ collisional dimer (aka O$_4$) observed at 20° elevation angle is correlated

456 with the lofted DOFS (Supplemental Figure S6). From this correlation we find that observations of clear

457 sky conditions have 20° elevation angle O$_4$ dSCD > 10^{43} molecule^{2}cm^{-5} and use this cut to distinguish

458 clear sky versus clouds. To assure that GEOS-Chem results are only compared to the clear-sky

459 observational data, we apply this clear sky screen to the measured modeled BrO$_{LTcol}$ timeseries. The use

460 of this screen also assists in minimizing variability in the averaging kernels and thus allowing the April

461 averaged partial column averaging kernels (Figure 3) to be applied for clear skies at any time of the year.
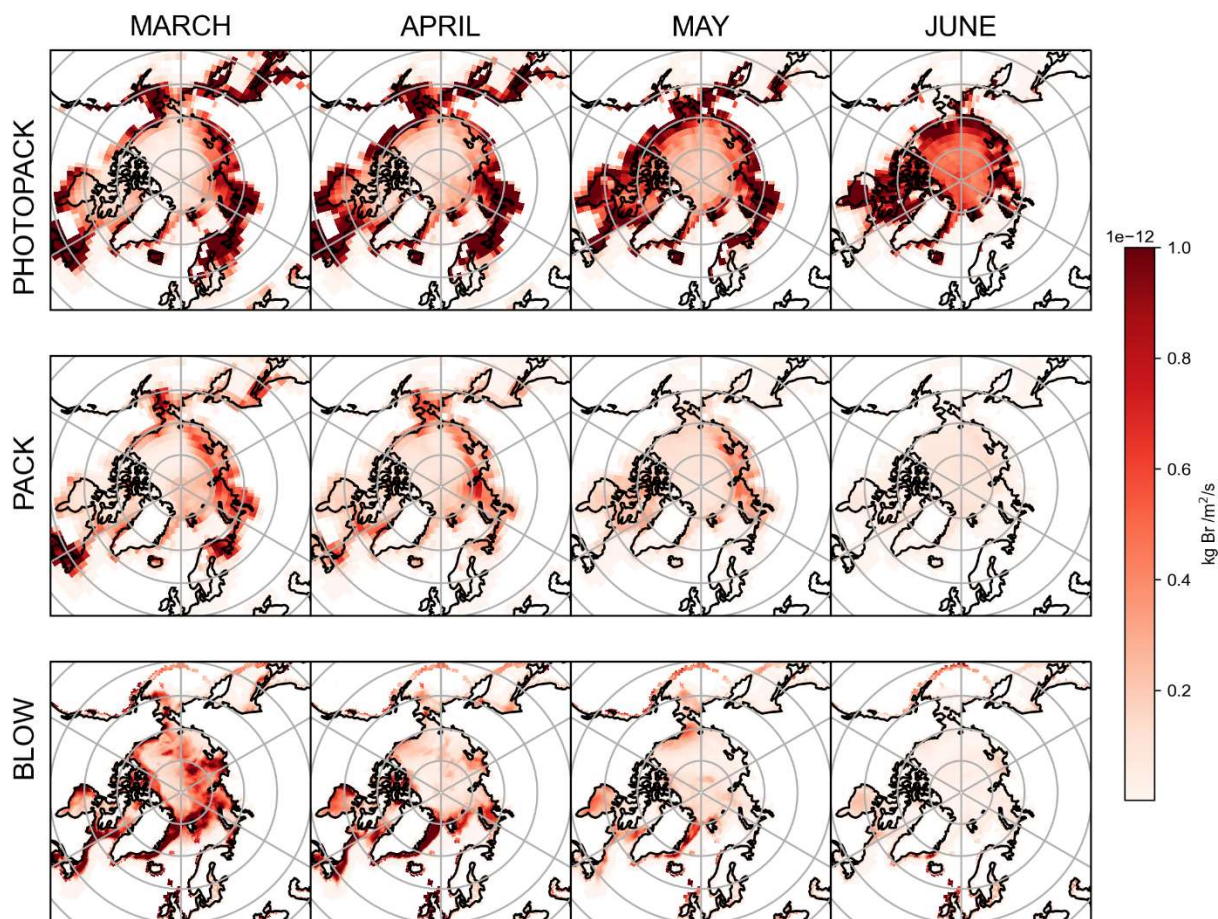
462

463 **Figure 4: Mean snowpack Br$_2$ emissions and p-Br$^-$ by month, as simulated by GEOS-Chem.**
464   The top row shows emissions of Br$_2$ in the PHOTOPACK run, the middle row shows the emissions of
465 Br$_2$ in the PACK run, and the bottom row shows emissions of p-Br$^-$ from adding the BLOW mechanism.
466 **3. Examining reactive bromine in the Arctic spring**

467 **3.1 Snowpack Br$_2$ emissions**
468   The top two rows of Figure 4 shows PHOTOPACK and PACK average snowpack Br$_2$ emissions
469 for each spring month. The emission of Br$_2$ in PHOTOPACK increases over the Arctic Ocean in May and

June, when the sun is above the horizon for up to 24 hours per day and ozone deposition yield is almost always at the photo-enhanced level of 7.5%. Notably, Br_2 emissions over the Arctic Ocean in the PHOTOPACK and BLOW+PHOTOPACK runs are highest in June when the sun is nearly always five degrees above the horizon and surface temperatures may drop below freezing. The PACK emissions are lower than the PHOTOPACK Br_2 emissions by an order of magnitude and shows a seasonal cycle with a high BrO_{LTcol} in April and May with a decrease in May and June. While our ozone deposition velocities (see Supplemental Figure S5) over Arctic sea ice are much higher than previous estimates of an approximate magnitude of 0.01 cm/s (Toyota et al., 2011), the PHOTOPACK run highlights that a 75-fold increase in daytime Br_2 yield can lead to predictions of increased Br_2 production over the North Pole in June. Monthly satellite observations show that BrO reaches a minimum over the Arctic Ocean in June (Richter et al., 1998).

Coastal land regions within 200 km of the coastline have some of the highest modeled snowpack Br_2 emissions (see Figure 4 rows 1 and 2). ~~Dry deposition velocities are lower over ice covered ocean than open ocean due to the higher likelihood of a stable surface boundary layer over the ice-covered ocean (Toyota et al., 2016). This remains true within~~Within GEOS-Chem, ~~as~~ deposition rates are greatest over land, less rapid over ice-covered ocean, and lowest over open ocean (see Supplemental Figure S5). Lower dry deposition velocities over the ice-covered Arctic Ocean lead to decreased deposition and conversion to Br_2. In GEOS-Chem, ozone mixing ratios and deposition are over three orders of magnitude larger than $BrNO_3$ and HOBr mixing ratios and deposition over the Arctic Ocean, and ozone deposition contributes more than half of total Br_2 emitted in the PACK and BLOW+PACK runs. Our snowpack mechanism assumes that all ozone deposited to the surface of a grid cell reacts with the snowpack cover and produces Br_2. This assumption is more appropriate in the barren snow-covered coastal tundra but may be less accurate in areas where deposition to vegetation dominates. This nonconservative approach may lead to overestimation of Br_2 emissions from snowy vegetated surfaces. Our screens for snowpack emissions described in section 1.3.5 tried to minimize these effects but may not work perfectly due to finite grid cell resolution and other challenges. Increased Br_2 emissions observed in Figure 4 in northern Europe may also be partially driven by increased local mixing ratios of ozone and NO_x over industrialized regions such as the Kola Peninsula.

3.2 Blowing ~~s~~Snow ~~pBr~~ aerosol bromide ~~-~~emissions

The bottom row of Figure 4 shows the total quantity of particulate bromide released by the blowing snow SSA mechanism in the BLOW runs. Emissions over the Arctic Ocean decline each month after the March maximum as rising temperatures increase the ~~windspeed~~wind speed threshold for blowing snow SSA production. Some icy coastal regions with frequently high ~~windspeed~~wind speeds such as the

503   Aleutian Islands south of Alaska and the eastern coast of Greenland continue to emit SSA p-Br⁻ in April,

504   and the extremely high winds in the Aleutians enable SSA production into May. The location of specific

505   high-wind storm systems in spring 2015 may be evident in the darker red spots over the Arctic Ocean,

506   which are particularly noticeable over the Eurasian and Central Arctic in March. These monthly averages

507   are only accurate for the months in spring 2015 and may not be spatially representative of blowing snow

508   SSA production in other years.

509   The impact of the blowing snow SSA emissions on measured BrO is minimal on O-Buoys in the

510   Beaufort Gyre, possibly due to the spatial and seasonal variations in SSA p-Br⁻ emissions. Figure 4 shows

511   that 2015 SSA production was highest in March and April on the Eurasian and Central sector of the

512   Arctic, and thus the O-Buoys deployed as shown in Figure 2 are less exposed to the effects of SSA

513   production than the Arctic as a whole. Particulate bromide must be activated from SSA by heterogeneous

514   reactions as in Figure 1 and Table 3, leading to photochemical cycles that sustain further activation of

515   bromide from SSA. The dearth of sunlight over the Arctic Ocean in early March coincides with the

516   greatest SSA p-Br⁻ production and means that the increased February SSA p-Br⁻ emissions may not lead to

517   a direct increase in BrO.

518
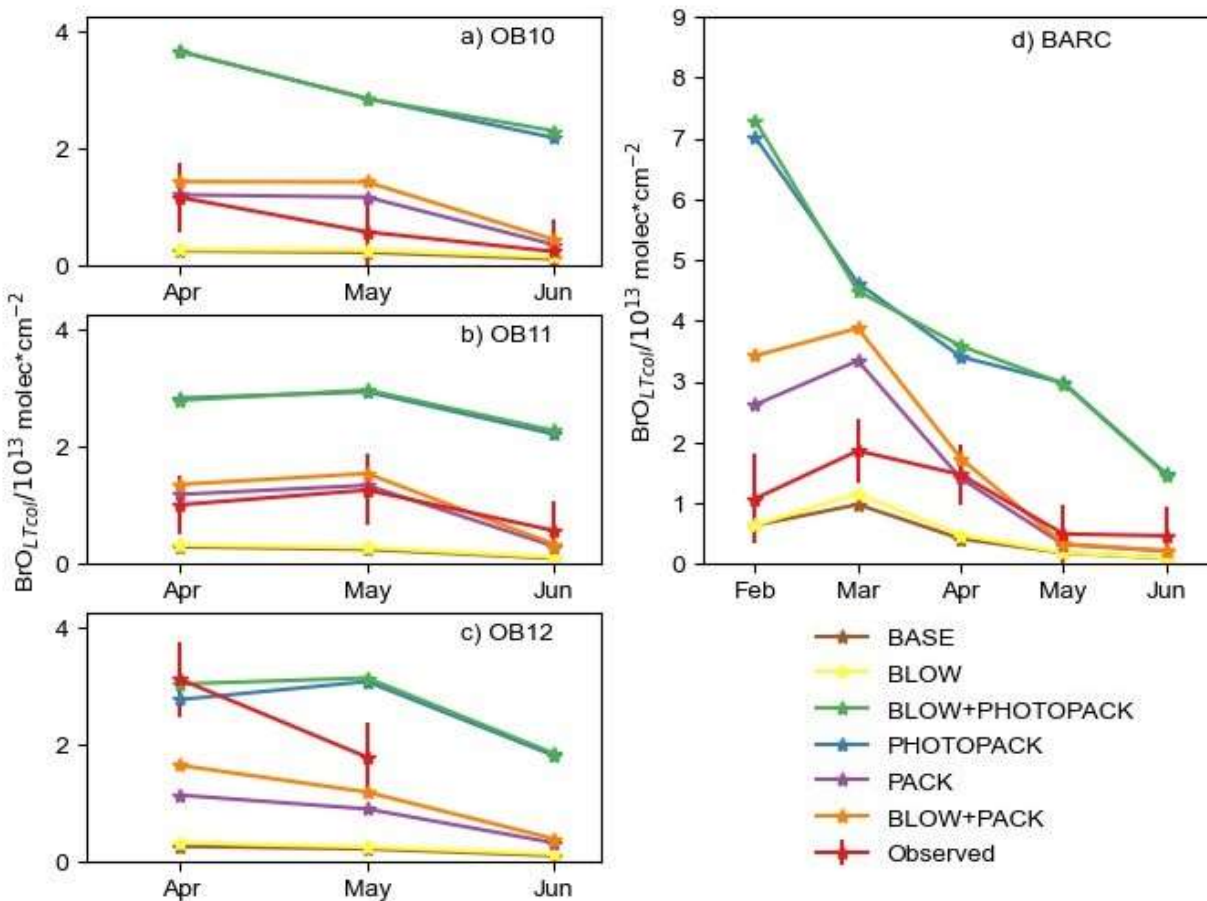
Figure 5: Monthly average BrO$_{LTcol}$ in observations and model

Monthly averages of BrO at a) O-Buoy 10, b) O-Buoy 11, c) O-Buoy 12, and d) BARC at Utqiaġvik only using predictions and observations when dSCDO$_4$ >1*10^{43} molecules^{2}cm^{-5}. Observations with average 1σ error shown in red. All units in 10^{13} molecules/cm^2.

3.3 Snowpack Br$_2$ emissions have more impact than blowing snow SSA on monthly BrO abundance

Increased levels of bromine have been historically seen at Utqiaġvik during February, March, April and May (Berg et al., 1983). Previous O-Buoy data analysis noted BrO dropping to zero in June (Burd et al., 2017). Figure 5 shows monthly averaged modeled BrO$_{LTcol}$ at Utqiaġvik and on the O-Buoys for each model configuration. The difference in GEOS-Chem modeled monthly averaged BrO$_{LTcol}$ for O-Buoys is minimal between the BASE and BLOW runs, the PHOTOPACK and BLOW+PHOTOPACK runs, and the PACK and BLOW+PACK runs.

Both BASE and BLOW runs predict near-zero BrO$_{LTcol}$ on all O-Buoys and during most months at Utqiaġvik. The exception to this is the slight increases in monthly modeled BrO$_{LTcol}$ to 1*10^{13} molecules/cm^2 in March and April. This BASE increase in BrO$_{LTcol}$ indicates that oceanic SSA rather than blowing snow SSA can affect modeled BrO at Utqiaġvik due to its closer proximity to open ocean regions

535 than the O-Buoys. The increases in BrO from the BASE model due to the addition of BLOW, most

536 evident at Utqiaġvik in March 2015, are a result of increased particulate bromide available for activation

537 on aerosol surfaces. The PACK and BLOW+PACK runs show the highest skill in reproducing

538 observations, falling within the monthly average of hourly measured BrO_{LTcol} error for 9 of the 13 months

539 plotted in Figure 5. Both PACK and BLOW+PACK replicate the observed monthly pattern on O-Buoy 11

540 and at Utqiaġvik especially well. The seasonal pattern of maximum modeled BrO_{LTcol} at Utqiaġvik in

541 March followed by a decrease to near-zero modeled BrO_{LTcol} in May is replicated in both runs despite the

542 overprediction of BrO_{LTcol} in February and March. The BLOW+PACK monthly BrO_{LTcol} is between

543 $1*10^{124}$ molecules/cm^2 and $1*10^{13}$ molecules/cm^2 higher than PACK monthly BrO_{LTcol} due to the addition

544 of blowing snow SSA. This increase is most pronounced in February and March at Utqiaġvik when lower

545 temperatures lead to lower threshold ~~windspeed~~wind speeds and increased SSA production (see

546 Supplemental Figure S4).

547   The inclusion of increased daytime yield of snowpack Br_2 drives monthly average BrO_{LTcol} above

548 $3*10^{13}$ molecules/cm^2 in the PHOTOPACK and BLOW+PHOTOPACK runs from February until June,

549 far above peak observed monthly BrO_{LTcol} of $2*10^{13}$ molecules/cm^2. The PHOTOPACK and

550 BLOW+PHOTOPACK runs show steady decline in BrO_{LTcol} from February to June at Utqiaġvik.

551 Predictions of PHOTOPACK and BLOW+PHOTOPACK monthly June BrO_{LTcol} above $2*10^{13}$

552 molecules/cm^2 on the O-Buoys is due to increasing photo-assisted local snowpack Br_2 emissions over the

553 Arctic Ocean (see Figure 5). The PHOTOPACK mechanism predicts monthly average BrO_{LTcol} within

554 observational error only on O-Buoy 12 in April. Aside from this replication of the sparsely sampled O-

555 Buoy 12 April BrO_{LTcol}, the PHOTOPACK mechanism overestimates BrO_{LTcol}. ~~This overprediction of~~

556 ~~BrO_{LTcol} by PHOTOPACK and BLOW+PHOTOPACK extends to prediction of unrealistically high~~

557 ~~mixing ratios for all tropospheric bromine species (see Supplemental Figure S7). This overprediction is a~~

558 ~~product of high ozone deposition velocities and daytime conversion rates to Br_2.~~

559
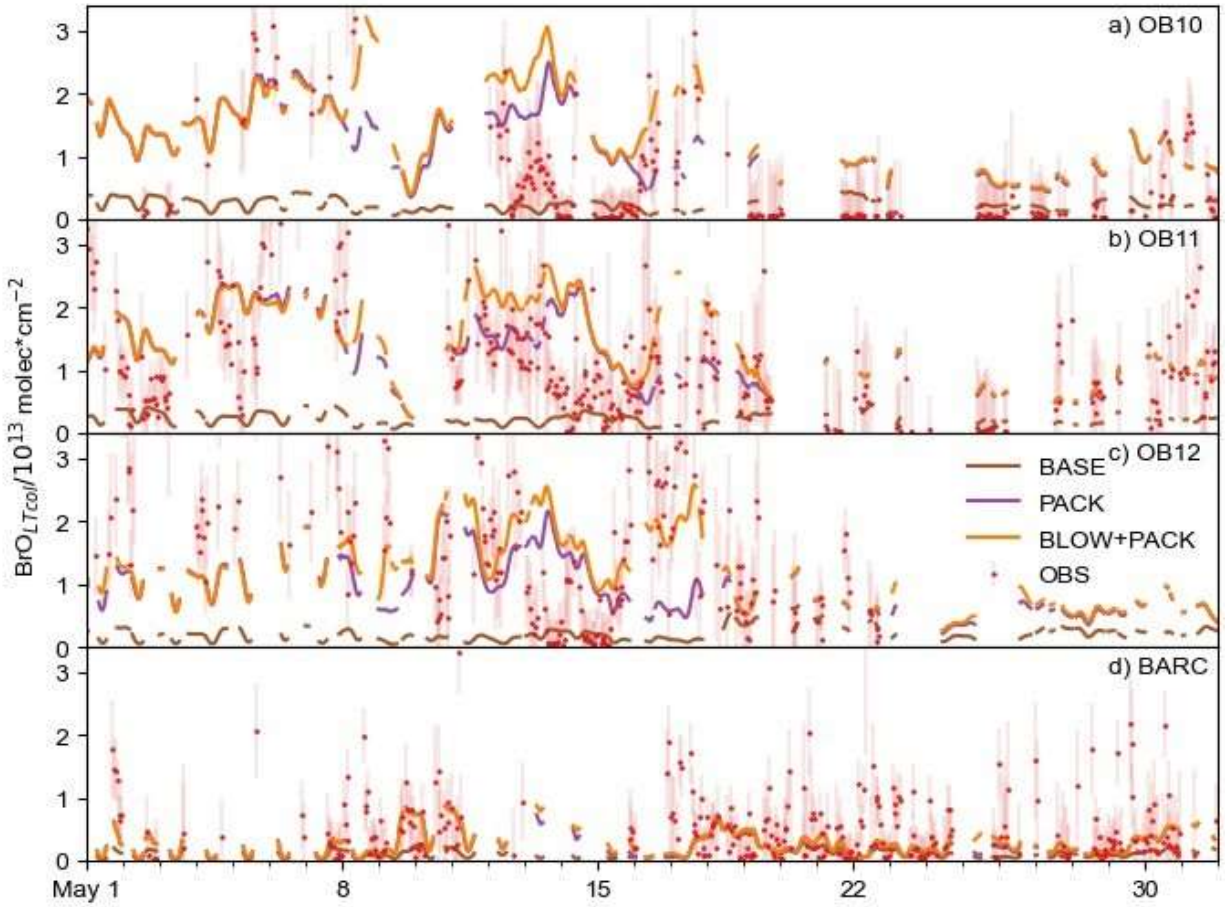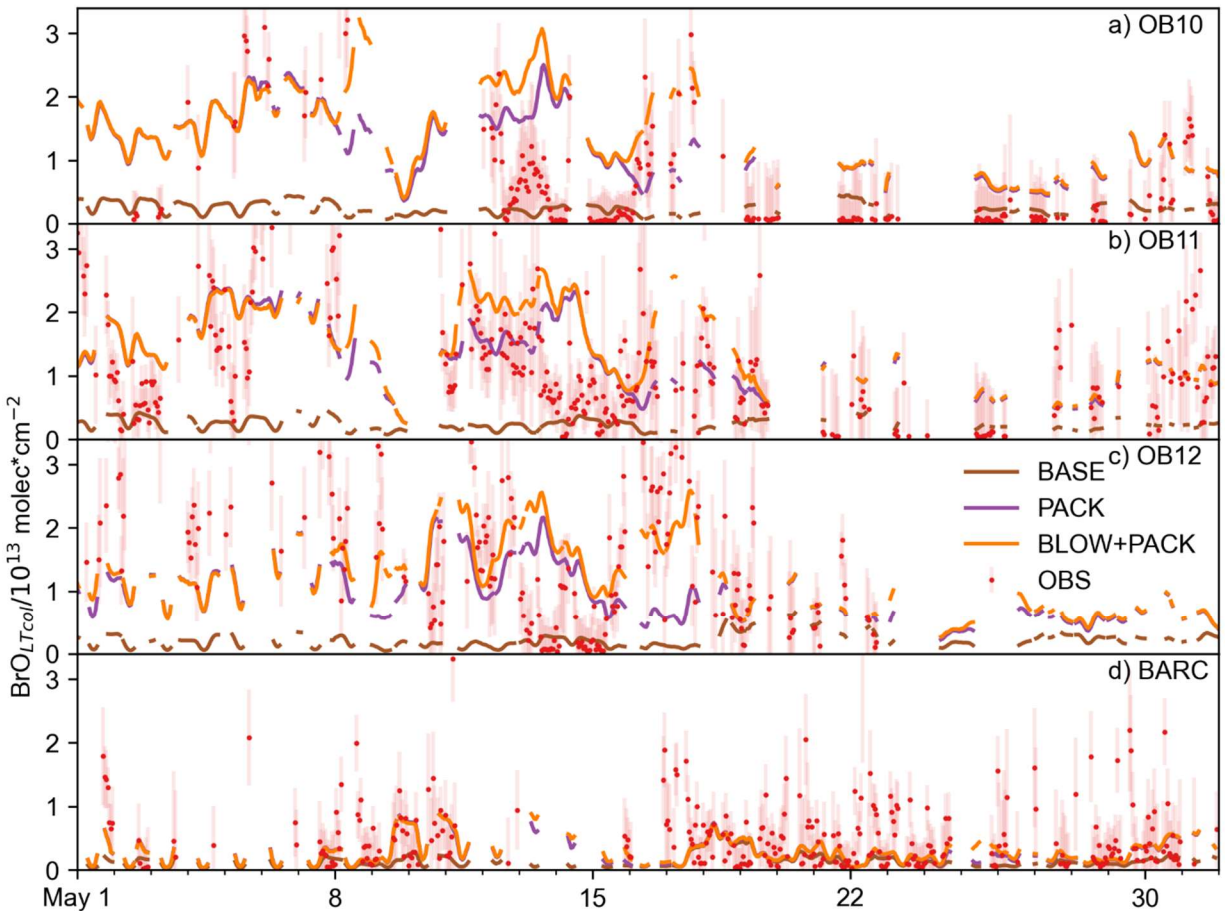
Figure 6: May Hourly BrO$_{LTcol}$ timeseries

Hourly timeseries of BLOW+PACK, PACK, and BASE BrO$_{LTcol}$ on a) O-Buoy 10, b) O-Buoy 11, c) O-Buoy 12 and d) BARC at Utqiaġvik in the 2015 Arctic Spring. O Buoy observations and error bars in red, BASE BrO$_{LTcol}$ in brown, PACK BrO$_{LTcol}$ in purple, and BLOW+PACK BrO$_{LTcol}$ in orange. All BrO$_{LTcol}$ plotted continuously except for gaps where dSCDO$_4$ >1*10^{43} molecules^{2}cm^{-5}.

3.4 BLOW+PACK run best replicates hourly BrO events in mid and late May

The model's hourly predictions of BrO$_{LTcol}$ in May 2015 are shown in Figure 6 for the BASE, PACK, and BLOW+PACK runs. Figure 6 screens modeled BrO$_{LTcol}$ for times when dSCD O^4 >1*10^{43} molecules^{2}cm^{-5}, while Supplemental Figures S7 and S8 make only direct comparisons between observations of BrO$_{LTcol}$ on the O-Buoys (S7) and at Utqiaġvik (S8) throughout all of Spring 2015. The O-Buoys show fluctuations in observed BrO$_{LTcol}$ during May and show consistent increased columns of BrO$_{LTcol}$ from May 10 to May 20. The BASE run never rises above 10^{13} molecules/cm^2 and underpredicts most May hourly BrO$_{LTcol}$, although BASE predicts monthly BrO$_{LTcol}$ on OB10 for two out of three monthsMay and June. Both PACK and BLOW+PACK runs show bettermore skill in replicating BrO$_{LTcol}$. The addition of the snowpack mechanism allows us to predict increased BrO$_{LTcol}$ in late May on O-Buoys

577   10 and 11. This points to the role of surface snowpack in late-season events in agreement with the

578   findings of Burd et al. (2017).

579   We can identify the role of blowing snow SSA by comparing the PACK and BLOW+PACK runs.

580   Both PACK and BLOW+PACK runs underestimate BrO$_{LTcol}$ during the first ten days of May. BrO

581   predictions and ~~observations are more active~~show higher variability and peaks starting on May 10. The

582   blowing snow SSA mechanism increases BLOW+PACK BrO$_{LTcol}$ on May 12 and 13. PACK is skilled at

583   replicating observed O-Buoy 11 BrO$_{LTcol}$ on both days, and both PACK and BLOW+PACK are within

584   observational BrO$_{LTcol}$ error on May 13.

585   A BrO event also occurs on May 13 on O-Buoy 10. While the strength of the O-Buoy 10 BrO

586   event is overestimated by PACK and BLOW+PACK, the shape of that event is ~~duplicated~~reproduced in

587   both runs. ~~Examination of the O-Buoy 10 vertical Br$_y$ profile in Supplemental Figure S7 shows surface~~

588   ~~BrO increasing to 2 pmol/mol in the lowest 200 meters of the troposphere on May 10. BrO is mixed~~

589   ~~vertically on May 12 and 13 throughout the lower troposphere, with a linear decrease from surface BrO~~

590   ~~mixing ratios of 3 pmol/mol to 0 pmol/mol at 1200 m altitude. This May 12 BrO$_{LTcol}$ event is also~~

591   ~~associated with surface ozone depletion to 15 nmol/mol.~~

592   Observed BrO$_{LTcol}$ decreases rapidly on all O-Buoys after May 14, and the model is unable to

593   track this sharp decrease. Rapid changes in BrO$_{LTcol}$ may be caused by sharp edges in BrO-enriched

594   airmasses such as those seen by Simpson et al. (2017). GEOS-Chem run at this resolution cannot replicate

595   abrupt changes in BrO, but it does slowly decrease BrO$_{LTcol}$ to reach BrO$_{LTcol}$ to less than 10^{13}

596   molecules/cm^2 on May 16. The BLOW+PACK mechanism is skilled in replicating the magnitude and

597   features of a mid-May BrO event on ~~several~~ O-Buoys 10 and 11.

598   Figure 7 shows all Spring 2015 BrO$_{LTcol}$ observations on O-Buoys 10, 11, 12, and BARC plotted

599   against PACK BrO$_{LTcol}$ and BLOW+PACK BrO$_{LTcol}$. The increase in BrO$_{LTcol}$ on adding BLOW leads to

600   fewer underpredictions of observations (see bottom right section of Figure 7b). The Pearson correlation

601   coefficient (r) between PACK ~~GC~~BrO$_{LTcol}$ and observed BrO$_{LTcol}$ is 0.33, improving to 0.39 on addition of

602   BLOW in the BLOW+PACK run. Other runs show less skill in replicating observations, with a BASE

603   BrO$_{LTcol}$ Pearson correlation to observations of 0.19 and a BLOW BrO$_{LTcol}$ Pearson correlation to

604   observations of 0.23. We also performed a simple linear regression to determine the relationship between

605   predictions and observations for each run. The slope of the line of best fit improves drastically on addition

606   of PACK, changing from 0.06 for BASE and 0.07 for BLOW to 0.33 for PACK and 0.44 for

607   BLOW+PACK. There is a positive synergistic effect on the slope of the line of best fit when using both

608   BLOW and PACK in combination rather than individually. The use of both BLOW and PACK

609 mechanisms implements literature findings on the processes influencing Arctic reactive bromine and

610 increases correlation between GEOS-Chem predictions and observations.

611
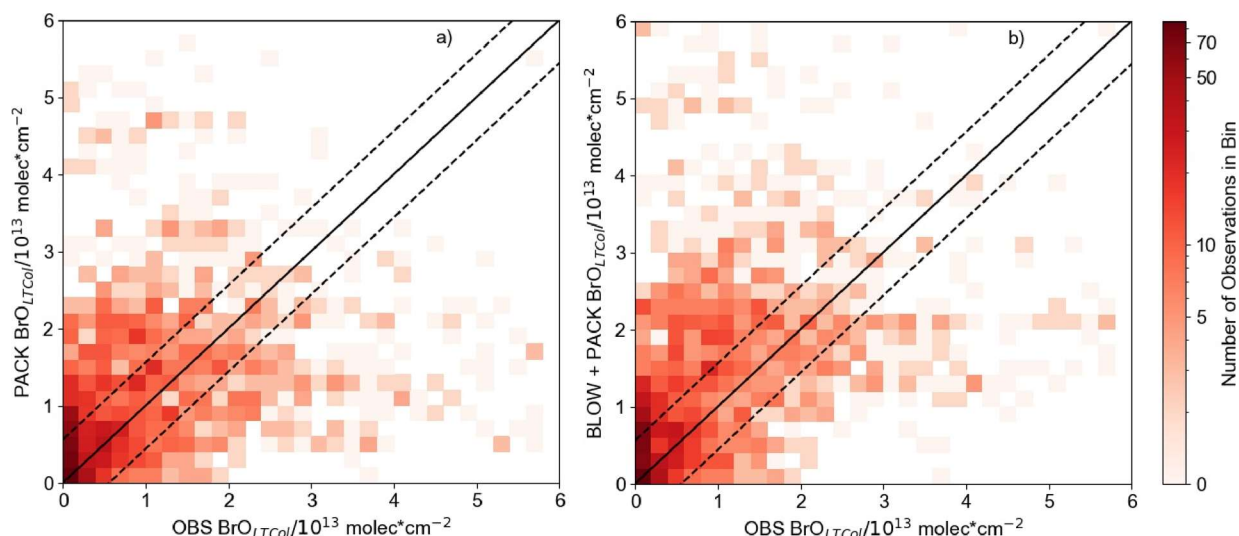
Figure 7: Hourly modeled BrO$_{LTcol}$ versus BrO$_{LTcol}$ observations
613 Two dimensional histograms showing density of GEOS-Chem predicted ~~BrO$_{LTcol}$ s~~BrO versus all
614 observed Spring 2015 hourly Br$_{LTcol}$, with a) PACK BrO$_{LTcol}$ shown at left sorted into square bins of 0.2
615 with an Pearson *r* correlation to observations of 0.33 and b) BLOW+PACK BrO$_{LTcol}$ on the bottom sorted
616 into square bins of 0.2 with Pearson *r* correlation to observations to 0.39. All units are in molecules/cm^2.
617 1:1 line drawn in the center in black, with a margin of the average observational error plotted in dashed
618 black lines around the central 1:1 line.

619 **4. Arctic Spring reactive bromine modeling discussion**

620 **4.1 Use of both mechanisms in conjunction leads to best prediction of tropospheric BrO results**

621   Table 2 shows the root mean squared error (RMSE) of each model run as compared to BrO$_{LTcol}$

622 observations in at each different location in Spring 2015. The PACK and BLOW+PACK runs have the

623 lowest RMSE on O-Buoys 11 and 12, and among the lowest RMSE on O-Buoy 10. Utqiaġvik shows the

624 lowest RMSE of 1.25*10^{13} molec/cm^2 for the BLOW run, although the PACK run is not too far off at

625 1.57*10^{13} molec/cm^2. Depiste the fact that BLOW+PACK has a higher RMSE of 1.75*10^{13} molec/cm^2 at

626 Utqiaġvik, the BLOW+PACK run performs the best or near the best of all runs on the O-Buoys and

627 includes both known processes for Arctic reactive bromine production. The PHOTOPACK and

628 BLOW+PHOTOPACK runs with increased daytime yield have a consistently high RMSE of 2.46*10^{13}

629 molec/cm^2 or higher, often double the RMSE of other model runs.

630   Initial implementation of this snowpack mechanism in Toyota et al. (2011) increased the daytime

631 yield of Br$_2$ from ozone ~~depletion~~ deposition to 7.5% to improve agreement between observed and

632 modeled surface ozone mixing ratios. Toyota et al. (2011) also increased the surface resistance of ozone

633 to 10^4~~000~~ s/m, decreased deposition velocities on Arctic snowpack to approximately 0.01 cm/s. Our

model using a constant yield of Br from ozone deposition performs best, despite observations that sunlight has an effect on reactive bromine recycling in the snowpack (Pratt et al., 2013; Custard et al., 2017). GEOS-Chem does not explicitly model heterogeneous photochemistry within the snowpack interstitial space but does include heterogeneous bromine chemistry on aerosol particle surfaces after the Br_2 is emitted from the snowpack into the lowest model layer. The updates to GEOS-Chem halogen chemistry (Schmidt et al., 2016; Sherwen et al., 2016b; Chen et al., 2017; Wang et al., 2019b) should be mechanistically sufficient to model daytime heterogeneous chemistry of reactive bromine on aerosol surfaces. We note that improvements to GEOS-Chem have increased the explicit modeling of these photochemical recycling and amplification processes, possibly reducing the need for empirical increases to daytime yields.

Our findings differ from recent implementations of the snowpack mechanism in Herrmann et al. (2021) and Marelle et al. (2021). While all snowpack mechanisms are based on Toyota et al. (2011), several large differences in model configuration and mechanism implementation explain these differences. We allow Br_2 production from ozone deposition over all snow surfaces, leading to much higher Br_2 production over MYI and coastal regions. Land snowpack can produce Br_2 on exposure to ozone and sunlight (Pratt et al., 2013; Custard et al., 2017) and Figure 4 shows our coastal snowpack producing large quantities of Br_2. Tropospheric reactive bromine chemistry has been observed up to 200 km inland from the coast (Peterson et al., 2018). Marelle et al. (2021) underestimates BrO in late March and overestimates Utqiaġvik BrO in early April. This seasonal pattern may be due to increased daytime ozone yield on first year ice near Utqiaġvik in April. Herrmann et al. (2021) found that HOBr and $BrNO_3$ deposition was more important in driving snowpack Br_2 production and that the daytime yield of 7.5% Br_2 on ozone deposition underpredicted BrO. We find that ozone contributes slightly more than HOBr and $BrNO_3$ because we allow for Br_2 production on ozone deposition over multi-year ice and coastal snowpack regions. The temporal scale of this manuscript spans the entire year, while Herrmann et al. (2021) only spans February, March, and April. Our longer timescale highlights the issue of increased daytime Br_2 yield during May and June (see Figure 4 PHOTOPACK) with increased emissions over the Arctic Ocean that are not in agreement with satellite observations of minimal Arctic tropospheric BrO in June (Richter et al., 1998).

Table 2: Model root mean square error by run and location.
Root mean squared model error (RMSE) shown in ~~pmol/mol~~ BrO$_{LTcol.}$/10^{12} molec/cm^2 RMSE calculated as the square root of the mean of the squared errors for all observations with valid BrO$_{LTcol}$ in Spring 2015.

Units in BrO$_{LTcol.}$/10^{12} molec/cm^2	OB10	OB11	OB12	Utqiaġvik~~UTQ~~
BASE	9.9	12.9	22.9	13.0
BLOW	9.7	12.7	22.4	12.5

PACK	9.9	10.0	18.6	15.2
BLOW+PACK	10.1	10.1	15.7	17.5
PHOTOPACK	30.0	24.8	26.2	30.1
BLOW+PHOTOPACK	30.3	24.6	26.3	31.4

666

4.2 Addition of PACK mechanism increases surface ozone predictive skill

The Barrow Arctic Research Center (BARC) in Utqiaġvik has the most comprehensive coverage of surface ozone in Spring 2015. A constant yield of 0.1% Br_2 from ozone deposition allows us to approximate the average vertical extent of ozone depletion events at Utqiaġvik in May 2015. The increase in Br_y in the PACK and BLOW+PACK runs is confined to the lowest 1000 m of the atmosphere (see Supplemental Figure S97). Ozone depletions, caused by reactive bromine chemistry, often only occur within the lowest 1000 m of the troposphere (Bottenheim et al., 2002; Salawitch et al., 2010). Previous studies have found evidence of lofted BrO in plumes at altitudes up to 900 m AGL (Peterson et al., 2017). The monthly average Utqiaġvik May surface ozone in BLOW and BLOW+PACK is 22 nmol/mol, matching mean May surface ozone from 1999-2008 (Oltmans et al., 2012). The PHOTOPACK runs generate mean May surface ozone depletion to approximately 5 nmol/mol, far below the May mean. The PACK and BLOW+PACK runs duplicate the approximate vertical extent of elevated bromine levels and the strength of typicalhistoric May ozone depletion.

Figure 8 shows hourly ozone predictions alongside BARC ozone observations (McClure-Begley, Petropavlovskikh, and Oltmans, 2014). The BASE model fails to replicate variance in ozone measured at BARC in Utqiaġvik, with a Pearson correlation coefficient to observations of 0.35. Adding PACK improves Pearson correlation to 0.47, within rounding error of BLOW+PACK Pearson correlation of 0.47. Both PACK and BLOW+PACK significantly improve model performance in replicating ozone depletions in such as the depletion below 30 nmol/mol from March 20 to March 29 but fail to track the subsequent recovery of ozone to background levels on April 1. Predicted PACK ozone does not recover to backgrounds levels up to theuntil a height of roughly 1000 m. A similar pattern where our model replicates low ozone but fails to predict the recovery of ozone to background levels occurs on April 5 and 15. Examination of ozone profiles in GEOS-Chem found that GEOS-Chem underpredicts tropospheric ozone by 10-20 ppb north of 60° latitude (Wang et al., 2021), which contributes to the low ozone predictions in our runs. Previous modeling of Utqiaġvik spring 2012 ozone in WRF-Chem found a similar linear correlation coefficient of 0.5 to BROMEX observations (Simpson et al., 2017) when using both blowing snow and snowpack mechanisms (Marelle et al., 2021). We are biased low compared to observations, with a root mean square error of 17.0 nmol/mol in BLOW+PACK compared to a root mean square error of 12.9 nmol/mol in Marelle et al. (2021). This may be partially due to limited vertical resolution in GEOS-Chem that may be inadequate to describe shallow surface-based temperature

697   inversions and subsequent recovery. The high bias in ozone deposition velocity over sea ice surfaces may

698   also contribute to low ozone mixing ratios near the surface.

699
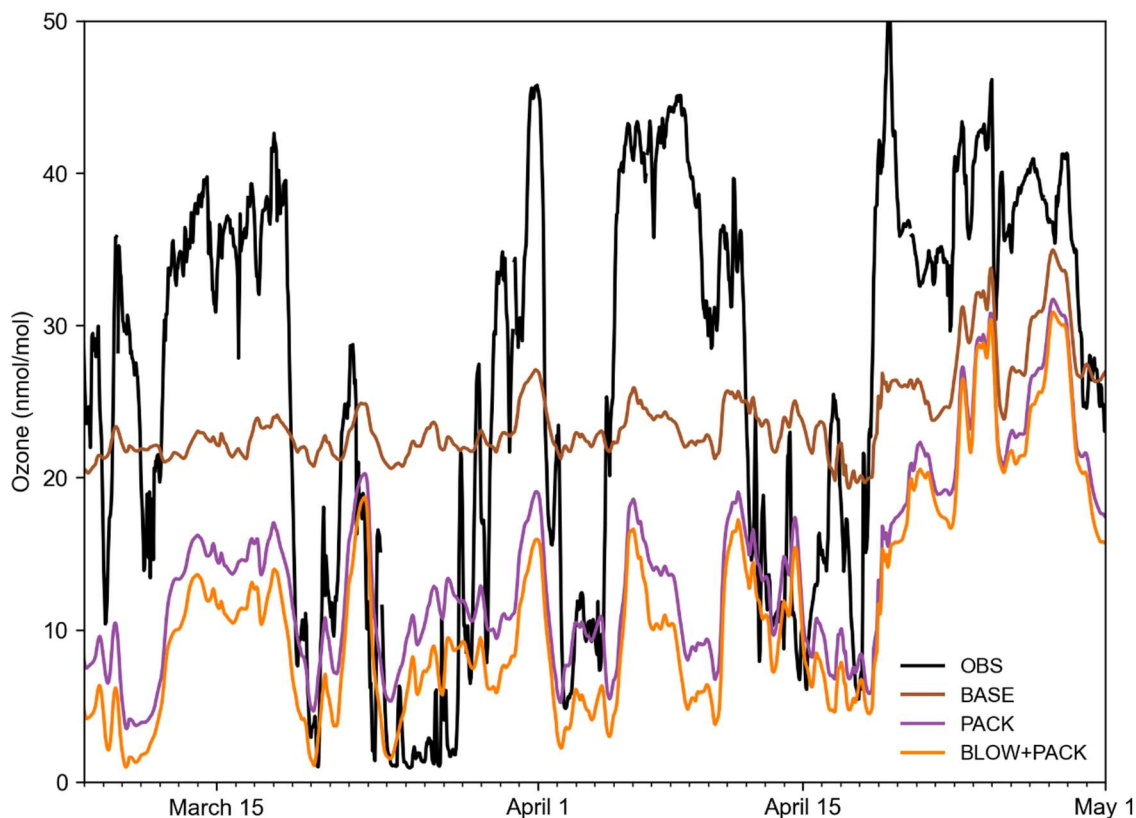
Figure 8: Hourly Utqiaġvik ozone timeseries
Hourly timeseries of BLOW+PACK, PACK, and BASE ozone at Utqiaġvik in the 2015 Arctic Spring.
Ozone observations at BARC in black (McClure-Begley, Petropavlovskikh and Oltmans, 2014), BASE
ozone in brown, PACK ozone in purple, and BLOW+PACK ozone in orange. Gaps indicate missing
observational data.

        A similar improvement in ozone predictions on the addition of PACK is seen on the O-Buoys, but

is harder to quantify due to observational gaps in ozone data. Supplemental Figure S10 shows hourly

ozone predictions graphed over O-Buoy 11 observations and Supplemental Figure S11 shows hourly

ozone predictions graphed over O-Buoy 12. O-Buoy 10 was not able to gather an observations of ozone in

2015. The clearest impact of PACK in Figures S10 and S11 is seen in early April, with observed ozone

dropping near zero nmol/mol and PACK and BLOW+PACK runs dropping to five nmol/mol while the

BASE run remains near 20 nmol/mol. Figure S10 shows that ozone predictions on O-Buoy 10 in May are

less accurate, failing to fall below 10 nmol/mol ozone while observations show ozone dropping near the

detection limit. The O-Buoys appear to experience more late-season ozone depletion events that GEOS-

715 Chem fails to replicate, possibly due to warming temperatures increasing vertical mixing and replenishing

716 ozone near the surface.

717

718 **Table 3: Arctic Tropospheric Reactions Rates by Model Run**

719 Rates for each of the reactions listed in Figure 1 organized by GEOS-Chem run. All units are listed as

720 millions of moles per hour across the region shown in Supplemental Figure S14. R in equation R2 refers

721 to any organic molecule. Y in equation 1 represents NO, Cl, or H. X in equation HR6a represents either

722 Br or Cl. PHOTOPACK and BLOW+PHOTOPACK are excluded as they severely overpredict BrO as

723 seen in Figures 4 and 5.

	BASE	BLOW	PACK	BLOW+PACK	Reaction Equation
R1	17.57	17.77	27.7	28.4	$BrO + YO \rightarrow Br + O_2$
R2	236.28	261.75	435.74	472.14	$Br + O_3 \rightarrow BrO + O_2$
R3	0.7	0.84	1.38	1.54	$Br + RH \rightarrow HBr, Br + HO_2 \rightarrow HBr$
R4	0.01	0.01	0.02	0.02	$HBr + OH \rightarrow Br + H_2O$
R5	9.41	9.47	14.41	14.01	$BrO + HO_2 \rightarrow HOBr$
R6	1.63	2.4	12.78	16.16	$BrO + BrO \rightarrow Br_2 + O_2$
R7	0.03	0.06	0.04	0.06	$BrO + ClO \rightarrow BrCl + O_2$
R8	2.8	2.94	5.69	5.86	$BrO + NO_2 \rightarrow BrNO_3$
R9	0	0	0	0	$Br_2 + OH \rightarrow Br + HOBr$
R10	0.15	0.17	1.39	1.64	$Br + BrNO_3 \rightarrow Br_2 + NO_3$
R11	0.18	0.18	0.55	0.7	$Br + NO_2 \rightarrow BrNO_2$
HR1a	0.04	0.03	0.15	0.1	$HOBr + HBr \rightarrow Br_2 + H_2O$
HR1b	0.79	0.95	1.47	1.68	$HOBr + p\text{-}Br^- \rightarrow Br_2 + OH^-$
HR2	0.17	0.21	0.38	0.38	$HOBr + H_2O + HSO_3^- \rightarrow H_2SO_4 + HBr + OH^-$
HR3	0.25	0.29	0.43	0.44	$BrNO_3 + H_2O \rightarrow HNO_3 + HOBr$
HR4a	0	0	0	0	$HBr + O_3 \rightarrow HOBr + O_2$
HR4b	0.07	0.09	0.14	0.15	$p\text{-}Br^- + O_3 + H_2O \rightarrow HOBr + O_2 + OH^-$
HR5	0	0	0	0	$BrNO_3 + HCl \rightarrow BrCl + HNO_3$
HR6a	0	0	0	0	$HOX + HX \rightarrow BrCl + H_2O$
HR6b	0.29	0.54	0.37	0.68	$HOBr + p\text{-}Cl^- \rightarrow BrCl + OH^-$
HR7a	0	0	0	0	$HBr + ClNO_x \rightarrow BrCl + HNO_x$
HR7b	0	0	0	0	$p\text{-}Br^- + ClNO_x + H_2O \rightarrow BrCl + HNO_x + OH^-$
HR8	0	0	0	0	$p\text{-}Br^- + IO_x > IBr + O_x$
P1	1.38	1.76	6.04	7.24	$Br_2 + hv \rightarrow 2Br$
P2	203.54	227.07	362.89	392.04	$BrO + hv \rightarrow Br + O$
P3	8.45	8.11	12.6	11.75	$HOBr + hv \rightarrow OH + Br$
P4	0.36	0.37	0.57	0.56	$BrNO_3 + hv \rightarrow BrO + NO_2$
P5	2.04	2.1	3.24	3.17	$BrNO_3 + hv \rightarrow Br + NO_3$
P6	0.18	0.18	0.55	0.7	$BrNO_2 + hv \rightarrow Br + NO_2$
P7	0.35	0.63	0.45	0.76	$BrCl + hv \rightarrow Br + Cl$
P8	0	0	0	0	$BrI + hv \rightarrow Br + I$

724

5.   Examining reactive bromine in the Arctic in September and October

725

726   O-Buoys deployed during fall 2015 measured BrO slant column densities characterized by noise

727   around zero (see Supplemental Figures S12~~8~~ and S13~~9~~). We do not retrieve vertical column density from

728   these fall slant column densities, because the resulting retrievals would be biased positive due to an

729   algorithm requirement that only positive BrO column densities are allowed in the optimal estimation

730   inversion. These differential slant column densities (dSCDs) can be used qualitatively to determine the

731   presence or absence of BrO above the detection limit. If the d~~C~~SCDs display noise around zero at all

732   viewing angles, the BrO in the troposphere is below the detection limit of the spectrometer. ~~The~~ A pattern

733   of larger BrO dSCDs at near-horizon viewing elevation angles indicating the presence of tropospheric

734   BrO above the detection limit is only observed at Utqiaġvik during Arctic Spring (see ~~in 2015~~

735   Supplemental Figure S12~~7~~)~~, indicate the presence of tropospheric BrO above the detection limit, which~~

736   ~~only occur during Arctic spring~~. Any BrO present in the Arctic troposphere in September and October

737   falls below detection limits at Utqiaġvik (see Supplemental Figure S12~~8~~) and on each O-Buoy (see

738   Supplemental Figure S13~~9~~). The average Arctic Spring 2015 MAX-DOAS BrO_{LTcol} detection limits are 5

739   x 10^{12} molecules/cm^2 (Peterson et al., 2015; Simpson et al., 2017; Swanson et al., 2020). Both BLOW and

740   PACK mechanisms lead to prediction of increased fall BrO because the weather and sea ice conditions

741   specified in the emission algorithms occur in fall as well as spring.

742   Figure 9 shows fall predictions of BrO_{LTcol} filtered for times when solar elevation angle was

743   greater than 5˚. BASE and ~~SNOW~~ PACK BrO_{LTcol} remain near zero in September but rise above the

744   MAX-DOAS detection limit of 5 x10^{12} molecules/cm^2 BrO_{LTcol} in October. The addition of the blowing

745   snow SSA mechanism propels BLOW BrO_{LTcol} up to 6 x 10^{13} molecules/cm^2 in October. O-Buoys 13 and

746   14 have the highest modeled fall BrO_{LTcol} but even Utqiaġvik has several days of BrO_{LTcol} above 5 x10^{12}

747   molecules/cm^2 in late October. There is no clear evidence of any BrO above MAX-DOAS detection limits

748   at Utqiaġvik or on any O-Buoy in October, as seen by the dSCDs scattered around zero in Supplemental

749   Figures S12~~8~~ and S13~~9~~.

750

751
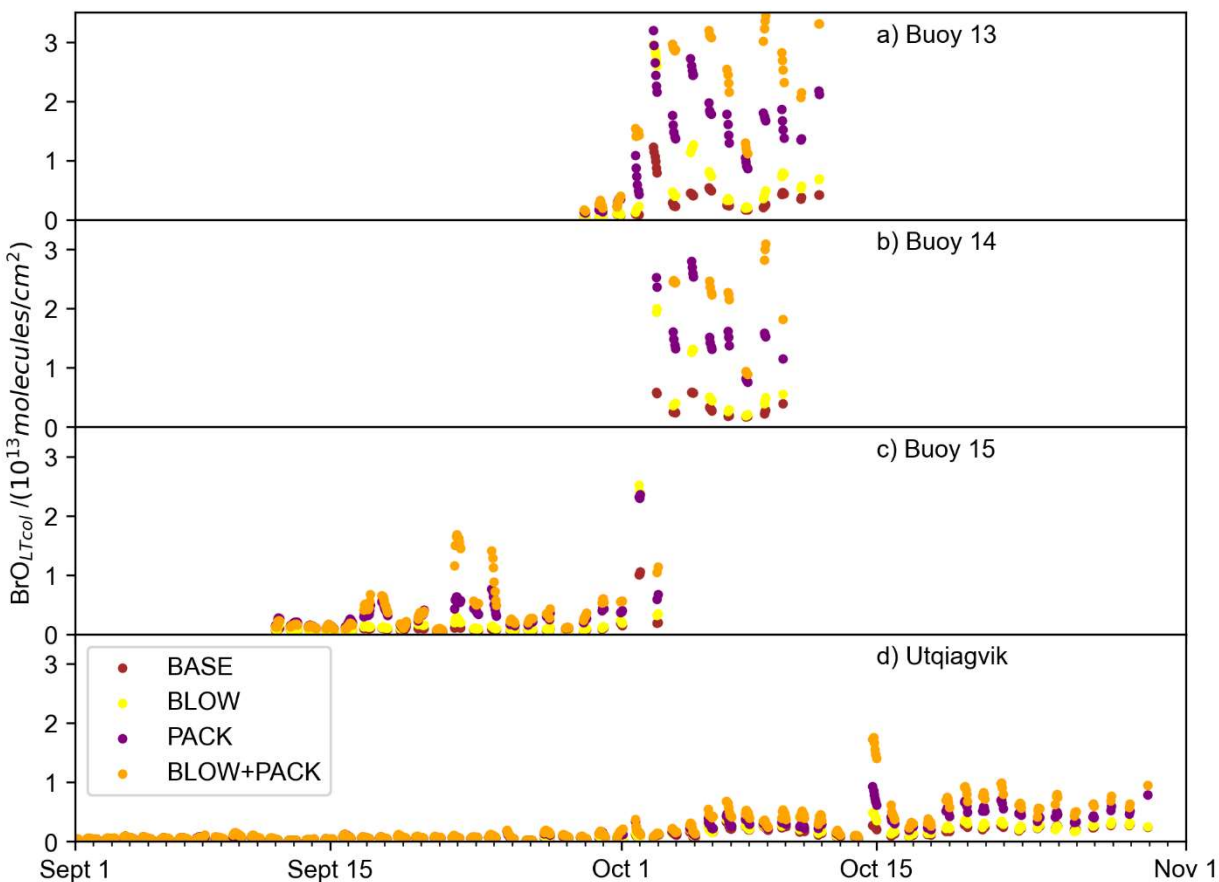
Figure 9: Fall GEOS-Chem Predicted BrO$_{LTcol}$
Hourly timeseries of BLOW+PACK, PACK, and BASE BrO$_{LTcol}$ on a) O-Buoy 10, b) O-Buoy 11, c) O-
Buoy 12 and d) BARC at Utqiaġvik during September and October 2015 BASE BrO$_{LTcol}$ in brown,
BLOW BrO$_{LTcol}$ in yellow, PACK BrO$_{LTcol}$ in purple, and BLOW+PACK BrO$_{LTcol}$ in orange. All BrO$_{LTcol}$
plotted continuously except for gaps where solar elevation angle was less than 5˚.

Both mechanisms assume that snowpack and SSA are just as capable of recycling reactive

bromine as in the springtime. High fall and winter SSA agrees with observations of peak SSA during

polar winter in both Antarctica (Wagenbach et al., 1998) and in the Arctic (Jacobi et al., 2012). The

deposition of Arctic haze (Douglas and Sturm, 2004) and SSA (Jacobi et al., 2019) increases snowpack

salinity and sulfate content over the course of winter and spring. This seasonal change in snowpack

salinity and acidity may enable reactive bromine recycling in the Arctic Spring, but there may not

sufficient haze and SSA deposition in fall to decrease snowpack pH and increase snowpack bromide

content. Additional observations of fall snowpack over sea ice including ion content could show different

snowpack composition in spring and fall. Thus the GEOS-Chem model overestimates fall BrO by

assuming the fall snowpack is equally capable of reactive bromine recycling as spring snowpack, possibly

due to the assumption of an infinite reservoir of snowpack bromide in all seasons. Most other modeling

exercises have focused on spring with unknown predictions in fall, possibly indicating problems in

769 mechanisms or parameterizations being employed, so we suggest that modeling should be done for a full

770 year to improve underlying chemistry and physics. We also suggest a fall snow sampling campaign to

771 validate modeled fall BrO.

6. Conclusions

773   We add snowpack Br_2 production to GEOS-Chem based on multiple field observations

774 demonstrating molecular bromine production in snowpack interstitial air. We use a mechanistic

775 parameterization of snowpack Br_2 production based on Toyota et al. (2011) in which Br_2 is emitted from

776 all snowpack of sufficient salinity and depth over land and sea ice upon deposition of the precursor

777 species HOBr, $BrNO_3$, and ozone. Prior work has also added a blowing snow SSA production mechanism

778 that increases aerosol particulate bromide and thus facilitates heterogeneous recycling of reactive bromine

779 on these aerosol particle surfaces. We update the halogen scheme to GEOS-Chem 12.9.3 and performed

780 six model simulations including a BASE run with neither blowing snow SSA nor snowpack emissions, a

781 PACK run assuming constant yield of Br_2 on ozone deposition over all snow surfaces, a PHOTOPACK

782 run assuming increased daytime yield of Br_2 on ozone deposition (similar in Toyota et al., 2011), a

783 BLOW run using only blowing snow SSA formation and two additional runs combing BLOW and each

784 respective PACK mechanism. The increased daytime yield of Br_2 in PHOTOPACK leads to

785 overprediction of BrO in these simulations, but the PACK run (with constant Br_2 yield day and night)

786 matches monthly averaged BrO vertical column densities within measurement error for 9 of 13 cases at

787 O-Buoy and Utqiagvik in springtime months. The PACK and BLOW+PACK runs were successful in

788 replicating observed mid May BrO events on O-Buoys in May. as well as recurrence events at the end of

789 May . The BLOW mechanism effectively increases aerosol surface available for turnover of reactive

790 bromine. The snowpack mechanism has more impact on modeled BrO mixing ratios than the blowing

791 snow SSA mechanism, but both contribute to tropospheric reactive bromine. We extend our model run to

792 the full year and find that enhanced daytime Br_2 yield can lead to increased Arctic Ocean Br_2 production

793 in the summer. Examining modeled BrO in fall 2015 reveals prediction of BrO when using these

794 mechanisms that are at odds with observations.

795   The inclusion of two Arctic reactive bromine production mechanisms based on literature

796 observations of snowpack Br_2 emission and blowing snow SSA formation improves model skill in

797 replicating Arctic tropospheric BrO in spring 2015. The snowpack is an important source of reactive

798 bromine, and SSA particles provide an abundant surface for sustained reactive bromine recycling in the

799 troposphere. We find that using both snowpack and blowing snow SSA bromine production mechanisms

800 is necessary for modeling BrO in the Arctic.

801 *Competing interests:* The authors declare that they have no conflict of interest.

Author contributions. WFS, WRS and CH designed the study. WRS collected and curated MAX-DOAS data. KC, LM, JT, LJ, JH and contributed code for reactive bromine mechanisms. CH, KC, LJ, JH, BA, SZ, QC, XW, and TS contributed model updates. WFS carried out modeling and analysis. WFS wrote the paper with input from all authors.

7. Acknowledgements

We acknowledge support from the National Science Foundation for providing funding under grants ARC-1602716, AGS-1702266, AGS-2109323, and ARC-1602883. This work also supported by the CNRS INSU LEFE-CHAT program under the grant Brom-Arc, and NASA grant 80NSSC19K1273. This research has received funding from the European Union's Horizon 2020 research and innovation program under grant agreement no. 689443 via project iCUPE (Integrative and Comprehensive Understanding on Polar Environments). The O-Buoy and Utqiagvik ground-based BrO datasets are available in the arcticdata.io repository (doi:10.18739/A2WD4W). We recognize the work of Jiayue Huang in adding the blowing snow SSA mechanism to GEOS-Chem. We would like to thank the National Oceanic and Atmospheric Administration (NOAA) Global Monitoring Division for the provision of ozone and temperature data near Utqiaġvik available online at doi:10.7289/V57P8WBF. We acknowledge use of the coastline distance dataset from the Pacific Islands Ocean Observing System. We acknowledge the use of imagery from the Land Atmosphere Near Real-Time Capability for EOS (LANCE) system and services from the Global Imagery Browse Services (GIBS), both operated by the NASA/GSFC/Earth Science Data and Information System (ESDIS, https://earthdata.nasa.gov) with funding provided by NASA/HQ. We owe a debt of gratitude to all members of the Atmospheric Chemistry and Global Change group at Florida State University for their support for working with GEOS-Chem and Python. We thank the global GEOS-Chem community for their tireless work to improve the model. We also thank all involved in the O-Buoy project for data collection and analysis.

8. References

Alexander, B., Park, R. J., Jacob, D. J., Li, Q. B., Yantosca, R. M., Savarino, J., Lee, C. C. W. and Thiemens, M. H.: Sulfate formation in sea-salt aerosols: Constraints from oxygen isotopes, J. Geophys. Res. D Atmos., 110(10), 1–12, doi:10.1029/2004JD005659, 2005.

AMAP: Arctic Monitoring and Assessment Program 2011: Mercury in the Arctic., 2011.

Artiglia, L., Edebeli, J., Orlando, F., Chen, S., Lee, M. T., Corral Arroyo, P., Gilgen, A., Bartels-Rausch, T., Kleibert, A., Vazdar, M., Andres Carignano, M., Francisco, J. S., Shepson, P. B., Gladich, I. and Ammann, M.: A surface-stabilized ozonide triggers bromide oxidation at the aqueous solution-vapour interface, Nat. Commun., 8(1), 1–7, doi:10.1038/s41467-017-00823-x, 2017.

Bariteau, L., Helmig, D., Fairall, C. W., Hare, J. E., Hueber, J. and Lang, E. K.: Determination of oceanic ozone deposition by ship-borne eddy covariance flux measurements, Atmos. Meas. Tech., 3(2), 441–455, doi:10.5194/amt-3-441-2010, 2010.

837 Barrie, L. A., Bottenheim, J. W., Schnell, R. C., Crutzen, P. J. and Rasmussen, R. A.: Ozone destruction
838 and photochemical reactions at polar sunrise in the lower Arctic atmosphere, Nature, 334(6178), 138–
839 141, doi:10.1038/334138a0, 1988.

840 Berg, W. W., Sperry, P. D., Rahn, K. A. and Gladney, E. S.: Atmospheric Bromine in the Arctic, J.
841 Geophys. Res., 88(3), 6719–6736, doi:10.1029/JC088iC11p06719, 1983.

842 Bey, I., Jacob, D. J., Yantosca, R. M., Logan, J. A., Field, B. D., Fiore, A. M., Li, Q., Liu, H. Y., Mickley,
843 L. J. and Schultz, M. G.: Global modeling of tropospheric chemistry with assimilated meteorology:
844 Model description and evaluation, J. Geophys. Res. Atmos., 106(D19), 23073–23095,
845 doi:10.1029/2001JD000807, 2001.

846 Bottenheim, J. W., Fuentes, J. D., Tarasick, D. W. and Anlauf, K. G.: Ozone in the Arctic lower
847 troposphere during winter and spring 2000 (ALERT2000), Atmos. Environ., 36, 2535–2544, 2002.

848 Burd, J. A., Peterson, P. K., Nghiem, S. V., Perovich, D. K. and Simpson, W. R.: Snow Melt Onset
849 Hinders Bromine Monoxide Heterogeneous Recycling in the Arctic, J. Geophys. Res. Atmos., 1–13,
850 doi:10.1002/2017JD026906, 2017.

851 Cao, L., Platt, U. and Gutheil, E.: Role of the boundary layer in the occurrence and termination of the
852 tropospheric ozone depletion events in polar spring, Atmos. Environ., 132, 98–110,
853 doi:10.1016/j.atmosenv.2016.02.034, 2016.

854 Carlson, D., Donohoue, D., Platt, U. and Simpson, W. R.: A low power automated MAX-DOAS
855 instrument for the Arctic and other remote unmanned locations, Atmos. Meas. Tech., 429–439, 2010.

856 Chance, K.: Analysis of BrO Measurements from the Global Ozone Monitoring Experiment, Geophys.
857 Res. Lett., 25(17), 3335–3338, 1998.

858 Chen, Q., Schmidt, J. A., Shah, V., Jaeglé, L., Sherwen, T. and Alexander, B.: Sulfate production by
859 reactive bromine: Implications for the global sulfur and reactive bromine budgets, Geophys. Res. Lett.,
860 44(13), 7069–7078, doi:10.1002/2017GL073812, 2017.

861 Choi, S., Wang, Y., Salawitch, R. J., Canty, T., Joiner, J., Zeng, T., Kurosu, T. P., Chance, K., Richter,
862 A., Huey, L. G., Liao, J., Neuman, J. A., Nowak, J. B., Dibb, J. E., Weinheimer, A. J., Diskin, G.,
863 Ryerson, T. B., Da Silva, A., Curry, J., Kinnison, D., Tilmes, S. and Levelt, P. F.: Analysis of satellite-
864 derived Arctic tropospheric BrO columns in conjunction with aircraft measurements during ARCTAS and
865 ARCPAC, Atmos. Chem. Phys., 12(3), 1255–1285, doi:10.5194/acp-12-1255-2012, 2012.

866 von Clarmann, T. and Glatthor, N.: The application of mean averaging kernels to mean trace gas
867 distributions, Atmos. Meas. Tech. Discuss., 1–11, doi:10.5194/amt-2019-61, 2019.

868 Clemer, K., Van Roozendael, M., Fayt, C., Hendrick, F., Hermans, C., Pinardi, G., Spurr, R., Wang, P.
869 and Maziere, M. De: Multiple wavelength retrieval of tropospheric aerosol optical properties from
870 MAXDOAS measurements in Beijing, Atmos. Meas. Tech., 3, 863–878, doi:10.5194/amt-3-863-2010,
871 2010.

872 Custard, K. D., Raso, A. R. W., Shepson, P. B., Staebler, R. M. and Pratt, K. A.: Production and Release
873 of Molecular Bromine and Chlorine from the Arctic Coastal Snowpack, ACS Earth Sp. Chem., 1, 142–
874 151, doi:10.1021/acsearthspacechem.7b00014, 2017.

875 Dery, S. J. and Yau, M. K.: A Bulk Blowing Snow Model, Bound. Layer Meteorol., 93, 237–251, 1999.

876 Déry, S. J. and Yau, M. K.: Simulation of blowing snow in the Canadian Arctic using a double-moment
877 model, Boundary-Layer Meteorol., 99(2), 297–316, doi:10.1023/A:1018965008049, 2001.

878   Domine, F., Sparapani, R., Ianniello, A. and Beine, H. J.: The origin of sea salt in snow on Arctic sea ice
879   and in coastal regions, Atmos. Chem. Phys. Discuss., 4(4), 4737–4776, doi:10.5194/acpd-4-4737-2004,
880   2004.

881   Douglas, T. A. and Sturm, M.: Arctic haze, mercury and the chemical composition of snow across
882   northwestern Alaska, Atmos. Environ., doi:10.1016/j.atmosenv.2003.10.042, 2004.

883   Eastham, S. D., Weisenstein, D. K. and Barrett, S. R. H.: Development and evaluation of the unified
884   tropospheric-stratospheric chemistry extension (UCX) for the global chemistry-transport model GEOS-
885   Chem, Atmos. Environ., 89, 52–63, doi:10.1016/j.atmosenv.2014.02.001, 2014.

886   Falk, S. and Sinnhuber, B. M.: Polar boundary layer bromine explosion and ozone depletion events in the
887   chemistry-climate model EMAC v2.52: Implementation and evaluation of AirSnow algorithm, Geosci.
888   Model Dev., 11(3), 1115–1131, doi:10.5194/gmd-11-1115-2018, 2018.

889   Fan, S. M. and Jacob, D. J.: Surface ozone depletion in Arctic spring sustained by bromine reactions on
890   aerosols, Nature, 359(6395), 522–524, doi:10.1038/359522a0, 1992.

891   Fischer, E. V., Jacob, D. J., Yantosca, R. M., Sulprizio, M. P., Millet, D. B., Mao, J., Paulot, F., Singh, H.
892   B., Roiger, A., Ries, L., Talbot, R. W., Dzepina, K. and Pandey Deolal, S.: Atmospheric peroxyacetyl
893   nitrate (PAN): A global budget and source attribution, Atmos. Chem. Phys., 14(5), 2679–2698,
894   doi:10.5194/acp-14-2679-2014, 2014.

895   Fisher, J. A., Jacob, D. J., Travis, K. R., Kim, P. S., Marais, E. A., Miller, C. C., Yu, K., Zhu, L.,
896   Yantosca, R. M., Sulprizio, M. P., Mao, J., Wennberg, P. O., Crounse, J. D., Teng, A. P., Nguyen, T. B.,
897   Clair, J. M. S., Cohen, R. C., Romer, P., Nault, B. A., Wooldridge, P. J., Jimenez, J. L., Campuzano-Jost,
898   P., Day, D. A., Hu, W., Shepson, P. B., Xiong, F., Blake, D. R., Goldstein, A. H., Misztal, P. K., Hanisco,
899   T. F., Wolfe, G. M., Ryerson, T. B., Wisthaler, A. and Mikoviny, T.: Organic nitrate chemistry and its
900   implications for nitrogen budgets in an isoprene- and monoterpene-rich atmosphere: Constraints from
901   aircraft (SEAC4RS) and ground-based (SOAS) observations in the Southeast US, Atmos. Chem. Phys.,
902   16(9), 5969–5991, doi:10.5194/acp-16-5969-2016, 2016.

903   Foster, K. L., Plastridge, R. A., Bottenheim, J. W., Shepson, P. B., Finlayson-pitts, B. J. and Spicer, C.
904   W.: The Role of Br 2 and BrCl in Surface Ozone Destruction at Polar Sunrise, Science (80-.).,
905   291(JANUARY), 471–475, 2001.

906   Frey, M. M., Norris, S. J., Brooks, I. M., Anderson, P. S., Nishimura, K., Yang, X., Jones, A. E.,
907   Nerentorp Mastromonaco, M. G., Jones, D. H. and Wolff, E. W.: First direct observation of sea salt
908   aerosol production from blowing snow above sea ice, Atmos. Chem. Phys., (April), 1–53,
909   doi:10.5194/acp-2019-259, 2020.

910   Frieß, U., Monks, P. S., Remedios, J. J., Rozanov, A., Sinreich, R., Wagner, T. and Platt, U.: MAX-
911   DOAS O4 measurements: A new technique to derive information on atmospheric aerosols: 2. Modeling
912   studies, J. Geophys. Res, 111, 20, doi:10.1029/2005JD006618, 2006.

913   Frieß, U., Beirle, S., Bonilla, L. A., Bösch, T., Friedrich, M. M., Hendrick, F., Piters, A., Richter, A.,
914   Roozendael, M. Van, Rozanov, V. V, Spinei, E. and Tirpitz, J.: Intercomparison of MAX-DOAS vertical
915   profile retrieval algorithms : studies using synthetic data, Atmos. Meas. Tech., (2), 2155–2181, 2019.

916   Gelaro, R., McCarty, W., Suarez, M. J., Todling, R., Molod, A., Takacs, L., Randles, C., Darmenov, A.,
917   Bosilovich, M., Reichle, R., Wargan, K., Coy, L., Cullather, R., Draper, C., Akella, S., Buchard, V.,
918   Conaty, A., Da Silva, A., Gu, W., Kim, G., Koster, R., Lucchesi, R., Merkova, D., Nielsen, J. E., Partyka,
919   G., Pawson, S., Putman, W., Rienecker, M., Schubert, S., Sienkiewicz, M. and Zhao, B.: The Modern-Era
920   Retrospective Analysis for Research and Applications , J. Clim., 30, 5419–5454, doi:10.1175/JCLI-D-16-
921   0758.1, 2017.

922   Group, N. O. B. P. and Stumpf, R.: Distance to Nearest Coastline: 0.01 Degree Grid, [online] Available
923   from: https://pae-paha.pacioos.hawaii.edu/thredds/ncss/dist2coast_1deg/dataset.html, 2021.

924   Halfacre, J. W., Knepp, T. N., Shepson, P. B., Thompson, C. R., Pratt, K. A., Li, B., Peterson, P. K.,
925   Walsh, S. J., Simpson, W. R., Matrai, P. A., Bottenheim, J. W., Netcheva, S., Perovich, D. K. and Richter,
926   A.: Temporal and spatial characteristics of ozone depletion events from measurements in the Arctic,
927   Atmos. Chem. Phys., 14(10), 4875–4894, doi:10.5194/acp-14-4875-2014, 2014.

928   Halfacre, J. W., Shepson, P. B. and Pratt, K. A.: pH-dependent production of molecular chlorine,
929   bromine, and iodine from frozen saline surfaces, Atmos. Chem. Phys, 19, 4917–4931, 2019.

930   Hara, K., Osada, K., Yabuki, M., Takashima, H., Theys, N. and Yamanouchi, T.: Important contributions
931   of sea-salt aerosols to atmospheric bromine cycle in the Antarctic coasts, Sci. Rep., 8(1),
932   doi:10.1038/s41598-018-32287-4, 2018.

933   Herrmann, M., Sihler, H., Frieß, U., Wagner, T., Platt, U. and Gutheil, E.: Time-dependent 3D
934   simulations of tropospheric ozone depletion events in the Arctic spring using the Weather Research and
935   Forecasting model coupled with Chemistry (WRF-Chem), , 7611–7638, 2021.

936   Holmes, C. D., Jacob, D. J., Corbitt, E. S., Mao, J., Yang, X., Talbot, R. and Slemr, F.: Global
937   atmospheric model for mercury including oxidation by bromine atoms, Atmos. Chem. Phys., 10(24),
938   12037–12057, doi:10.5194/acp-10-12037-2010, 2010.

939   Hönninger, G. and Platt, U.: Observations of BrO and its vertical distribution during surface ozone
940   depletion at Alert, Atmos. Environ., 36(15–16), 2481–2489, doi:10.1016/S1352-2310(02)00104-8, 2002.

941   Hönninger, G., von Friedeburg, C. and Platt, U.: Multi Axis Differential Optical Absorption Spectroscopy
942   (MAX-DOAS), Atmos. Chem. Phys., 4, 231–254, doi:10.5194/acpd-3-5595-2003, 2004.

943   Huang, J. and Jaeglé, L.: Wintertime enhancements of sea salt aerosol in polar regions consistent with a
944   sea-ice source from blowing snow, Atmos. Chem. Phys., (November), 1–23, doi:10.5194/acp-2016-972,
945   2017.

946   Huang, J., Jaeglé, L. and Shah, V.: Using CALIOP to constrain blowing snow emissions of sea salt
947   aerosols over Arctic and Antarctic sea ice, Atmos. Chem. Phys., 16253–16269, 2018.

948   Huang, J., Jaeglé, L., Chen, Q., Alexander, B., Sherwen, T., Evans, M., Theys, N. and Choi, S.:
949   Evaluating the impact of blowing snow sea salt aerosol on springtime BrO and O3 in the Arctic, Atmos.
950   Chem. Phys., 1–36, doi:10.5194/acp-2019-1094, 2020.

951   Jacobi, H. W., Voisin, D., Jaffrezo, J. L., Cozic, J. and Douglas, T. A.: Chemical composition of the
952   snowpack during the OASIS spring campaign 2009 at Barrow, Alaska, J. Geophys. Res. Atmos.,
953   doi:10.1029/2011JD016654, 2012.

954   Jacobi, H. W., Obleitner, F., Da Costa, S., Ginot, P., Eleftheriadis, K., Aas, W. and Zanatta, M.:
955   Deposition of ionic species and black carbon to the Arctic snowpack: Combining snow pit observations
956   with modeling, Atmos. Chem. Phys., 19(15), 10361–10377, doi:10.5194/acp-19-10361-2019, 2019.

957   Jaeglé, L., Quinn, P. K., Bates, T. S., Alexander, B. and Lin, J. T.: Global distribution of sea salt aerosols:
958   New constraints from in situ and remote sensing observations, Atmos. Chem. Phys., 11(7), 3137–3157,
959   doi:10.5194/acp-11-3137-2011, 2011.

960   Keller, C. A., Long, M. S., Yantosca, R. M., Da Silva, A. M., Pawson, S. and Jacob, D. J.: HEMCO v1.0:
961   A versatile, ESMF-compliant component for calculating emissions in atmospheric models, Geosci. Model
962   Dev., 7(4), 1409–1417, doi:10.5194/gmd-7-1409-2014, 2014.

Knepp, T. N., Bottenheim, J., Carlsen, M., Carlson, D., Donohoue, D., Friederich, G., Matrai, P. A., Netcheva, S., Perovich, D. K., Santini, R., Shepson, P. B., Simpson, W., Valentic, T., Williams, C. and Wyss, P. J.: Development of an autonomous sea ice tethered buoy for the study of ocean-atmosphere-sea ice-snow pack interactions: The O-buoy, Atmos. Meas. Tech., 3(1), 249–261, doi:10.5194/amt-3-249-2010, 2010.

Koo, J. H., Wang, Y., Kurosu, T. P., Chance, K., Rozanov, A., Richter, A., Oltmans, S. J., Thompson, A. M., Hair, J. W., Fenn, M. A., Weinheimer, A. J., Ryerson, T. B., Solberg, S., Huey, L. G., Liao, J., Dibb, J. E., Neuman, J. A., Nowak, J. B., Pierce, R. B., Natarajan, M. and Al-Saadi, J.: Characteristics of tropospheric ozone depletion events in the Arctic spring: Analysis of the ARCTAS, ARCPAC, and ARCIONS measurements and satellite BrO observations, Atmos. Chem. Phys., 12(20), 9909–9922, doi:10.5194/acp-12-9909-2012, 2012.

Krnavek, L., Simpson, W. R., Carlson, D., Domine, F., Douglas, T. A. and Sturm, M.: The chemical composition of surface snow in the Arctic: Examining marine, terrestrial, and atmospheric influences, Atmos. Environ., 50, 349–359, doi:10.1016/j.atmosenv.2011.11.033, 2012.

De Leeuw, G., Andreas, E. L., Anguelova, M. D., Fairall, C. W., Lewis, E. R., O'Dowd, C., Schulz, M. and Schwartz, S. E.: Production flux of sea spray aerosol, Rev. Geophys., 49(2), 1–39, doi:10.1029/2010RG000349, 2011.

Lehrer, E., Hönninger, G. and Platt, U.: A one dimensional model study of the mechanism of halogen liberation and vertical transport in the polar troposphere, Atmos. Chem. Phys., 4(11/12), 2427–2440, doi:10.5194/acp-4-2427-2004, 2004.

Lewis, E. R. and Schwartz, S. E.: Salt Aerosol Production: Mechanisms, Methods, Measurements, and Models: A Critical Review, American Geophysical Union, Washington D.C., 2004.

Lin, H., Jacob, D. J., Lundgren, E. W., Sulprizio, M. P., Keller, C. A., Fritz, T. M., Eastham, S. D., Emmons, L. K., Campbell, P. C., Baker, B., Saylor, R. D. and Montuoro, R.: Harmonized Emissions Component (HEMCO) 3.0 as a versatile emissions component for atmospheric models: Application in the GEOS-Chem, NASA GEOS, WRF-GC, CESM2, NOAA GEFS-Aerosol, and NOAA UFS models, Geosci. Model Dev., 14(9), 5487–5506, doi:10.5194/gmd-14-5487-2021, 2021.

Liu, T., Chan, A. W. H. and Abbatt, J. P. D.: Multiphase Oxidation of Sulfur Dioxide in Aerosol Particles: Implications for Sulfate Formation in Polluted Environments, Environ. Sci. Technol., acs.est.0c06496, doi:10.1021/acs.est.0c06496, 2021.

Mao, J., Paulot, F., Jacob, D. J., Cohen, R. C., Crounse, J. D., Wennberg, P. O., Keller, C. A., Hudman, R. C., Barkley, M. P. and Horowitz, L. W.: Ozone and organic nitrates over the eastern United States: Sensitivity to isoprene chemistry, J. Geophys. Res. Atmos., 118(19), 11256–11268, doi:10.1002/jgrd.50817, 2013.

Marelle, L., Thomas, J. L., Ahmed, S., Tuite, K., Stutz, J., Dommergue, A., Simpson, W. R., Frey, M. M. and Baladima, F.: Implementation and Impacts of Surface and Blowing Snow Sources of Arctic Bromine Activation Within WRF-Chem 4.1.1, J. Adv. Model. Earth Syst., 13(8), doi:10.1029/2020ms002391, 2021.

McClure-Begley, A. Petropavlovskikh, I. and Oltmans, S.: NOAA Global Monitoring Surface Ozone Network. 1973-2014. National Oceanic and Atmospheric Administration, Earth Systems Research Laboratory Global Monitoring Division. Boulder, CO, , doi:10.7289/V57P8WBF, 2014.

Mcnamara, S. M., Kolesar, K. R., Wang, S., Kirpes, R. M., May, N. W., Gunsch, M. J., Cook, R. D., Fuentes, J. D., Hornbrook, R. S., Apel, E. C., Laskin, A. and Pratt, K. A.: Observation of Road Salt Aerosol Driving Inland Wintertime Atmospheric Chlorine Chemistry, ACS Cent. Sci., 6(684–694),

doi:10.1021/acscentsci.9b00994, 2020.

Moore, C. W., Obrist, D., Steffen, A., Staebler, R. M., Douglas, T. A., Richter, A. and Nghiem, S. V: Convective forcing of mercury and ozone in the Arctic boundary layer induced by leads in sea ice., Nature, 506(7486), 81–4, doi:10.1038/nature12924, 2014.

Nghiem, S.: Studying bromine, ozone, and mercury chemistry in the Arctic, Eos, Trans. Am. Geophys. Union, 94(33), 289–291, doi:10.1038/NGEO1779., 2013.

Oltmans, S. J., Johnson, B. J. and Harris, J. M.: Springtime boundary layer ozone depletion at Barrow, Alaska: Meteorological influence, year-to-year variation, and long-term change, J. Geophys. Res. Atmos., 117(8), 1–18, doi:10.1029/2011JD016889, 2012.

Oum, K. W., Lakin, M. J. and Finlayson-Pitts, B. J.: Bromine activation in the troposphere by the dark reaction of O 3 with seawater ice, Geophys. Res. Lett., 25(21), 3923–3926, doi:10.1029/1998GL900078, 1998.

Parrella, J. P., Jacob, D. J., Liang, Q., Zhang, Y., Mickley, L. J., Miller, B., Evans, M. J., Yang, X., Pyle, J. A., Theys, N. and Van Roozendael, M.: Tropospheric bromine chemistry: Implications for present and pre-industrial ozone and mercury, Atmos. Chem. Phys., 12(15), 6723–6740, doi:10.5194/acp-12-6723-2012, 2012.

Peterson, P. K., Simpson, W. R., Pratt, K. A., Shepson, P. B., Frieß, U., Zielcke, J., Platt, U., Walsh, S. J. and Nghiem, S. V.: Dependence of the vertical distribution of bromine monoxide in the lower troposphere on meteorological factors such as wind speed and stability, Atmos. Chem. Phys., 15, 2119–2137, doi:10.5194/acp-15-2119-2015, 2015.

Peterson, P. K., Pöhler, D., Sihler, H., Zielcke, J., General, S., Frieß, U., Platt, U., Simpson, W. R., Nghiem, S. V., Shepson, P. B., Stirm, B. H., Dhaniyala, S., Wagner, T., Caulton, D. R., Fuentes, J. D. and Pratt, K. A.: Observations of bromine monoxide transport in the Arctic sustained on aerosol particles, Atmos. Chem. Phys., 17(12), 7567–7579, doi:10.5194/acp-17-7567-2017, 2017.

Peterson, P. K., Pöhler, D., Zielcke, J., General, S., Friess, U., Platt, U., Simpson, W. R., Nghiem, S., Shepson, P. B., Stirm, B. H. and Pratt, K. A.: Springtime Bromine Activation Over Coastal and Inland Arctic Snowpacks, ACS Earth Sp. Chem., acsearthspacechem.8b00083, doi:10.1021/acsearthspacechem.8b00083, 2018.

Peterson, P. K., Hartwig, M., May, N. W., Schwartz, E., Rigor, I., Ermold, W., Steele, M., Morison, J. H., Nghiem, S. V and Pratt, K. A.: Snowpack measurements suggest role for multi-year sea ice regions in Arctic atmospheric bromine and chlorine chemistry, Elementa, 2019.

Pöhler, D., Vogel, L., Friess, U. and Platt, U.: Observation of halogen species in the Amundsen Gulf, Arctic, by active long-path differential optical absorption spectroscopy., Proc. Natl. Acad. Sci. U. S. A., 107(15), 6582–7, doi:10.1073/pnas.0912231107, 2010.

Pound, R. J., Sherwen, T., Helmig, D., Carpenter, L. J. and Evans, M. J.: Influences of oceanic ozone deposition on tropospheric photochemistry, Atmos. Chem. Phys., 20(7), 4227–4239, doi:10.5194/acp-20-4227-2020, 2020.

Pratt, K. A., Custard, K. D., Shepson, P. B., Douglas, T. A., Pöhler, D., General, S., Zielcke, J., Simpson, W. R., Platt, U., Tanner, D. J., Gregory Huey, L., Carlsen, M. and Stirm, B. H.: Photochemical production of molecular bromine in Arctic surface snowpacks, Nat. Geosci., 6(5), 351–356, doi:10.1038/ngeo1779, 2013.

Richter, A., Wittrock, F., Eisinger, M. and Burrows, J. P.: GOME observations of tropospheric BrO in Northern Hemispheric spring and summer 1997, Geophys. Res. Lett., 25(14), 2683–2686,

doi:10.1029/98GL52016, 1998.

Rodgers, C. D. and Connor, B. J.: Intercomparison of remote sounding instruments, J. Geophys. Res., 108(March 2002), doi:10.1029/2002JD002299, 2003.

Saiz-Lopez, A. and von Glasow, R.: Reactive halogen chemistry in the troposphere, Chem. Soc. Rev., 41(19), 6448, doi:10.1039/c2cs35208g, 2012.

Salawitch, R. J., Canty, T., Kurosu, T., Chance, K., Liang, Q., Silva, A., Pawson, S., Nielsen, J. E., Rodriguez, J. M., Bhartia, P. K., Liu, X., Huey, L. G., Liao, J., Stickel, R. E., Tanner, D. J., Dibb, J. E., Simpson, W. R., Donohoue, D., Kreher, K., Johnston, P. V, Gao, R. S., Johnson, B., Bui, T. P. and Chen, G.: A new interpretation of total column BrO during Arctic spring, Geophys. Res. Lett., 37(21), 1–9, doi:10.1029/2010GL043798, 2010.

Sander, R., Keene, W. C., Pszenny, A. A. P., Arimoto, R., Ayers, G. P., Baboukas, E., Cainey, J. M., Crutzen, P. J., Duce, R. A., Hönninger, G., Huebert, B. J., Maenhaut, W., Mihalopoulos, N., Turekian, V. C. and Van Dingenen, R.: Inorganic bromine in the marine boundary layer: A critical review, Atmos. Chem. Phys., 3(5), 1301–1336, doi:10.5194/acp-3-1301-2003, 2003.

Schmidt, J. A., Jacob, D. J., Horowitz, H. M., Hu, L., Sherwen, T., Evans, M. J., Liang, Q., Suleiman, R. M., Oram, D. E., Le Breton, M., Percival, C. J., Wang, S., Dix, B. and Volkamer, R.: Modeling the observed tropospheric BrO background: Importance of multiphase chemistry and implications for ozone, OH, andmercury, J. Geophys. Res., 121(19), 11819–11835, doi:10.1002/2015JD024229, 2016.

Schroeder, W. H., Anlauf, K. G., Barrie, L. A., Lu, J. Y. and Steffen, A.: Arctic Springtime Depletion of Mercury, Nature, 394, 331–332, doi:10.1038/379126b0, 1998.

Shah, V., Jacob, D. J., Moch, J. M., Wang, X. and Zhai, S.: Global modeling of cloud water acidity , precipitation acidity , and acid inputs to ecosystems, Atmos. Chem. Phys, 12223–12245, 2020.

Sherwen, T., Schmidt, J. A., Evans, M. J., Carpenter, L. J., Großmann4, K., Eastham, S. D., J., D. J., Dix, B., Koenig, T. K., Sinreich, R., Ortega, I., Volkamer, R., Saiz-Lopez, A., Prados-Roman, C., Mahajan, A. S. and C. Ordóñez: DISCUSS Global impacts of tropospheric halogens (Cl, Br, I) on oxidants and composition in GEOS-Chem, Atmos. Chem. Phys. Discuss., (May), doi:10.5194/acp-2016-424, 2016a.

Sherwen, T., Schmidt, J. A., Evans, M. J., Carpenter, L. J., Großmann, K., Eastham, S. D., Jacob, D. J., Dix, B., Koenig, T. K., Sinreich, R., Ortega, I., Volkamer, R., Saiz-Lopez, A., Prados-Roman, C., Mahajan, A. S. and Ordóñez, C.: Global impacts of tropospheric halogens (Cl, Br, I) on oxidants and composition in GEOS-Chem, Atmos. Chem. Phys., 16(18), 12239–12271, doi:10.5194/acp-16-12239-2016, 2016b.

Sherwen, T., Evans, M. J., Carpenter, L. J., Schmidt, J. A. and Mickely, L. J.: Halogen chemistry reduces tropospheric O3 radiative forcing, Atmos. Chem. Phys., (August), 1–18, doi:10.5194/acp-2016-688, 2016c.

Simpson, W. R.: Atmospheric measurements via Multiple Axis Differential Optical Absorption Spectroscopy (MAXDOAS), Utqiagvik (Barrow), Alaska 2012-2018. Arctic Data Center, Arcticdata.io, doi:10.18739/A2222R550, 2018.

Simpson, W. R., Perovich, D. K., Matrai, P. A., Shepson, P. B. and Chavez, F.: The Collaborative O-Buoy Project: Deployment of a Network of Arctic Ocean Chemical Sensors for the IPY and beyond. Arctic Data Center, , doi:10.18739/A2WD4W, 2009.

Simpson, W. R., Brown, S. S., Saiz-Lopez, A., Thornton, J. A. and Glasow, R. Von: Tropospheric Halogen Chemistry: Sources, Cycling, and Impacts, Chem. Rev., 150312153236002, doi:10.1021/cr5006638, 2015.

Simpson, W. R., Peterson, P. K., Frieß, U., Sihler, H., Lampel, J., Platt, U., Moore, C., Pratt, K., Shepson, P., Halfacre, J. and Nghiem, S. V: Horizontal and vertical structure of reactive bromine events probed by bromine monoxide MAX-DOAS, Atmos. Chem. Phys., 17, 9291–9309, 2017.

Stutz, J., Thomas, J. L., Hurlock, S. C., Schneider, M., Von Glasow, R., Piot, M., Gorham, K., Burkhart, J. F., Ziemba, L., Dibb, J. E. and Lefer, B. L.: Longpath DOAS observations of surface BrO at Summit, Greenland, Atmos. Chem. Phys., 11(18), 9899–9910, doi:10.5194/acp-11-9899-2011, 2011.

Swanson, W. F., Graham, K. A., Halfacre, J. W., Holmes, C. D., Shepson, P. B. and Simpson, W. R.: Arctic Reactive Bromine Events Occur in Two Distinct Sets of Environmental Conditions : A Statistical Analysis of 6 Years of Observations Journal of Geophysical Research : Atmospheres, , 1–19, doi:10.1029/2019JD032139, 2020.

Tang, T. and McConnell, J. C.: Autocatalytic release of bromine from Arctic snow pack during polar sunrise, Geophys. Res. Lett., 23(19), 2633–2636, doi:10.1029/96GL02572, 1996.

Theys, N., Van Roozendael, M., Hendrick, F., Yang, X., De Smedt, I., Richter, A., Begoin, M., Errera, Q., Johnston, P. V., Kreher, K. and De Maziere, M.: Global observations of tropospheric BrO columns using GOME-2 satellite data, Atmos. Chem. Phys., 11(4), 1791–1811, doi:10.5194/acp-11-1791-2011, 2011.

Thomas, J. L., Stutz, J., Lefer, B., Huey, L. G., Toyota, K., Dibb, J. E. and Von Glasow, R.: Modeling chemistry in and above snow at Summit, Greenland - Part 1: Model description and results, Atmos. Chem. Phys., 11(10), 4899–4914, doi:10.5194/acp-11-4899-2011, 2011.

Toom-Sauntry, D. and Barrie, L. A.: Chemical composition of snowfall in the high Arctic: 1990-1994, Atmos. Environ., 36(15–16), 2683–2693, doi:10.1016/S1352-2310(02)00115-2, 2002.

Toyota, K., McConnell, J. C., Lupu, A., Neary, L., McLinden, C. A., Richter, A., Kwok, R., Semeniuk, K., Kaminski, J. W., Gong, S.-L., Jarosz, J., Chipperfield, M. P. and Sioris, C. E.: Analysis of reactive bromine production and ozone depletion in the Arctic boundary layer using 3-D simulations with GEM-AQ: inference from synoptic-scale patterns, Atmos. Chem. Phys., 11(8), 3949–3979, doi:10.5194/acp-11-3949-2011, 2011.

Toyota, K., Mcconnell, J. C., Staebler, R. M. and Dastoor, A. P.: Air – snowpack exchange of bromine , ozone and mercury in the springtime Arctic simulated by the 1-D model PHANTAS – Part 1 : In-snow bromine activation and its impact on ozone, Atmos. Chem. Phys., 4101–4133, doi:10.5194/acp-14-4101-2014, 2014.

Travis, K. R., Jacob, D. J., Fisher, J. A., Kim, P. S., Marais, E. A., Zhu, L., Yu, K., Miller, C. C., Yantosca, R. M., Sulprizio, M. P., Thompson, A. M., Wennberg, P. O., Crounse, J. D., St Clair, J. M., Cohen, R. C., Laughner, J. L., Dibb, J. E., Hall, S. R., Ullmann, K., Wolfe, G. M., Pollack, I. B., Peischl, J., Neuman, J. A. and Zhou, X.: Why do models overestimate surface ozone in the Southeast United States?, Atmos. Chem. Phys., 16(21), 13561–13577, doi:10.5194/acp-16-13561-2016, 2016.

Vogt, R., Crutzen, P. and Sander, R.: A mechanism for halogen release from sea-salt, Nature, 383(September), 327–331, 1996.

Wagenbach, D., Minikin, A., Ducroz, F., Mulvaney, R., Keck, L., Legrand, M., Hall, J. S. and Wolff, E. W.: Sea-salt aerosol in coastal Antarctic regions at three coastal, J. Geophys. Res. Atmos., 103, 961–974, 1998.

Wagner, T. and Platt, U.: Satellite mapping of enhanced BrO concentrations in the troposphere, Nature, 395(October), 486–490, doi:10.1038/26723, 1998.

Wang, S. and Pratt, K. A.: Molecular Halogens Above the Arctic Snowpack: Emissions, Diurnal

1136 Variations, and Recycling Mechanisms, J. Geophys. Res. Atmos., 122(21), 11,991-12,007,
1137 doi:10.1002/2017JD027175, 2017.

1138 Wang, S., Mcnamara, S. M., Moore, C. W., Obrist, D., Steffen, A., Shepson, P. B., Staebler, R. M., Raso,
1139 A. R. W. and Pratt, K. A.: Direct detection of atmospheric atomic bromine leading to mercury and ozone
1140 depletion, Proc. Natl. Acad. Sci., 116(29), doi:10.18739/A2D79598P.1, 2019a.

1141 Wang, X., Jacob, D. J., Eastham, S. D., Sulprizio, M. P., Zhu, L., Chen, Q., Alexander, B., Sherwen, T.,
1142 Evans, M. J., Lee, B. H., Haskins, J. D., Lopez-hilfiker, F. D., Thornton, J. A., Huey, G. L. and Liao, H.:
1143 The role of chlorine in global tropospheric chemistry, Atmos. Chem. Phys, 3981–4003, 2019b.

1144 Wang, X., Jacob, D. J., Downs, W., Zhai, S., Zhu, L., Shah, V., Holmes, C. D., Sherwen, T., Alexander,
1145 B., Evans, M. J., Eastham, S. D., Neuman, J. A., Veres, P. R., Koenig, T. K., Volkamer, R., Huey, L. G.,
1146 Bannan, T. J., Percival, C. J., Lee, B. H. and Thornton, J. A.: Global tropospheric halogen (Cl, Br, I)
1147 chemistry and its impact on oxidants, Atmos. Chem. Phys., 21(18), 13973–13996, doi:10.5194/acp-21-
1148 13973-2021, 2021.

1149 Wennberg, P. O.: Bromine explosion, Nature, 397(6717), 299–301, doi:10.1038/16805, 1999.

1150 Wren, S. N., Kahan, T. F., Jumaa, K. B. and Donaldson, D. J.: Spectroscopic studies of the heterogeneous
1151 reaction between O 3(g) and halides at the surface of frozen salt solutions, J. Geophys. Res. Atmos.,
1152 115(16), 1–8, doi:10.1029/2010JD013929, 2010.

1153 Wren, S. N., Donaldson, D. J. and Abbatt, J. P. D.: Photochemical chlorine and bromine activation from
1154 artificial saline snow, Atmos. Chem. Phys., 13(19), 9789–9800, doi:10.5194/acp-13-9789-2013, 2013.

1155 Yang, X., Pyle, J. A. and Cox, R. A.: Sea salt aerosol production and bromine release: Role of snow on
1156 sea ice, Geophys. Res. Lett., 35(16), 1–5, doi:10.1029/2008GL034536, 2008.

1157 Yang, X., Pyle, J. A., Cox, R. A., Theys, N. and Van Roozendael, M.: Snow-sourced bromine and its
1158 implications for polar tropospheric ozone, Atmos. Chem. Phys., 10(16), 7763–7773, doi:10.5194/acp-10-
1159 7763-2010, 2010.

1160 Yang, X., Frey, M., Rhodes, R., Norris, S., Brooks, I., Anderson, P., Nishimura, K., JOnes, A. and Wolff,
1161 E.: Sea salt aerosol production via sublimating wind-blown saline snow particles over sea ice:
1162 parameterizations and relevant microphysical mechanisms, Atmos. Chem. Phys., 19, 8407–8424, 2019.

1163 Zhu, L., Jacob, D. J., Eastham, S. D., Sulprizio, M. P., Wang, X., Sherwen, T., Evans, J., Chen, Q.,
1164 Alexander, B., Koenig, T. K., Volkamer, R. and Huey, L. G.: Effect of sea salt aerosol on tropospheric
1165 bromine chemistry, Atmos. Chem. Phys., 6497–6507, 2019.

1166